Mechanical Systems and Signal Processing 224 (2025) 112076

Contents lists available at ScienceDirect

Mechanical Systems and Signal Processing

journal homepage: www.elsevier.com/locate/ymssp

Improving unsupervised long-term damage detection in an uncontrolled environment through noise-augmentation strategy

Kang Yang [a,*], Chao Zhang [b], Hanbo Yang [a], Linyuan Wang [a], Nam H. Kim [c], Joel B. Harley [a,*]

[a] Department of Electrical and Computer Engineering, University of Florida, Gainesville, 32611, FL, USA
[b] Physics Department, University of Florida, Gainesville, 32611, FL, USA
[c] Department of Mechanical and Aerospace Engineering, University of Florida, Gainesville, 32611, FL, USA

ARTICLE INFO

Communicated by M. Rebillat

Keywords:
Structural health monitoring
Guided waves
Dynamic environments
Neural network
Noise augmentation
Unsupervised damage detection

ABSTRACT

Autoencoder reconstruction-based unsupervised damage detection is widely utilized in structural health monitoring. However, such methods typically necessitate a comprehensive collection of historical guided waves as training data. Acquiring such data presents challenges, as it requires prolonged monitoring to cover various environmental and operational conditions (EOCs), making these methods less practical for real-world applications. This paper proposes an unsupervised damage detection method solely trained on the current measurements directly. To improve the performance of the unsupervised damage detection method when the training data (the current measurements) contains a large ratio of damage-induced guided waves, two noise-augmentation strategies are designed to limit the neural network's learning ability to recover damage-induced guided waves from their segments, improving detection performance. Additionally, we use t-SNE to visualize the impact of noise augmentation on the separation of different types of guided waves within the recovery network's latent space. Experimental results indicate that input signals with relatively low SNR can achieve better damage detection performance, and a strategy for estimating the optimal noise intensity in input signals is provided in this paper. The effectiveness of the unsupervised this damage detection method with noise-augmentation strategy is validated by 10 regions of 80-days guided waves collected from uncontrolled and dynamic environmental conditions.

1. Introduction

A vast amount of infrastructure and mechanical systems, including bridges [1], pipelines [2], wind turbines [3], railway [4], and airplanes [5], undergo operational stresses throughout their lifespan, such as cyclic loadings and temperature variations. These stresses can lead to the onset and growth of fatigue damage, negatively impacting their functionality and potentially resulting in catastrophic structural failures [6]. To identify structural damage and estimate the remaining service life, these structures are outfitted with advanced structural health monitoring (SHM) systems. These systems rely on a network of permanently installed sensors on the structure to capture diagnostic signals. SHM systems may deploy hundreds of sensors to track environmental factors, like temperature and wind speed, as well as structural responses, such as acceleration, deflection, and strain [7]. With proper

* Corresponding authors.
E-mail addresses: yang.kang@ufl.edu (K. Yang), chao.zhang@ufl.edu (C. Zhang), yangh@ufl.edu (H. Yang), linyuanwang@ufl.edu (L. Wang), nkim@ufl.edu (N.H. Kim), joel.harley@ufl.edu (J.B. Harley).

https://doi.org/10.1016/j.ymssp.2024.112076
Received 19 April 2024; Received in revised form 20 September 2024; Accepted 18 October 2024
0888-3270/Published by Elsevier Ltd.

implementation, these techniques enable precise evaluations of structural safety and help avoid premature failures while minimizing unnecessary downtime [6,8].

In the field of structural health monitoring, damage diagnosis techniques based on ultrasonic guided waves (UGW) have garnered significant interest due to their notable advantages, including: (1) the ability to cover a large inspection area [8], (2) high sensitivity for detecting minor damages [9], and (3) the capacity for continuous, in-situ monitoring of structures in service [10]. Transducers are employed to emit and capture ultrasonic guided waves across the area under examination. Alterations in these ultrasonic guided waves are then employed to identify and pinpoint damage within the structures [11–13]. However, extracting reliable damage indicators from ultrasonic guided waves is fraught with difficulties due to the complex propagation characteristics of ultrasonic guided waves, such as dispersion, multimodality, and mode conversion. These challenges are accentuated in complex structures [6]. Furthermore, guided waves are susceptible to disturbances from variations in environmental and operational conditions (EOCs) [14–17], which include factors like temperature [14–16], humidity [18], flow rate [14], wind [18], and stress [17]. These conditions significantly complicate the task of detecting damage using guided waves in dynamic and complex scenarios [17].

To address the complexities of damage detection in variable environmental conditions, a variety of supervised learning methods have been introduced [19–22]. Although these techniques are effective in identifying, localizing, and quantifying damage, their heavy dependence on large, labeled datasets from both undamaged and differently damaged structures for training is a significant limitation. However, acquiring such datasets for complex or real-life structures often proves to be impractical due to the following several challenges: (1) collecting a diverse range of damage data for specific infrastructures, such as pipelines, bridges, and buildings, is challenging [23,24]; (2) each structure showcases distinct modal and mechanical features, owing to the variation in construction materials; (3) even structures that are alike in shape, size, and age exhibit unique boundary conditions [25,26]; (4) moreover, gathering labeled data is a strenuous, time-consuming, and costly endeavor, with the labeling process also vulnerable to human error, adding another layer of complexity [23]. These impediments severely limit the practical application of supervised machine learning and deep learning algorithms under complex conditions [23,27]. Hence, unsupervised machine learning approaches emerge as an effective alternative to surmount these significant challenges [28].

Among the various unsupervised damage detection techniques, deep learning models are particularly popular for their effectiveness in detecting damage without supervision. Instead of focusing solely on outlier data, such as guided waves caused by damage, researchers gather an abundance of signals from undamaged structures to develop unsupervised detection systems. These deep learning models, commonly employing autoencoders or similar architectures, are designed to learn the normal characteristics of the data. By training on healthy signals, these models can subsequently identify anomalies in test datasets by comparing reconstruction errors against predefined thresholds [29]. In the field of guided wave-based structural health monitoring (GW-SHM), researchers have explored deep learning-based unsupervised damage detection under lab-controlled dynamic conditions. Sawant et al. initially proposed a convolutional neural network (CNN)-based automated feature extraction framework combined with a Gaussian mixture model (GMM) for temperature compensation, damage classification, and localization. This supervised learning approach was tested on three types of damage (rivet hole, added mass, and notch) under simulated temperature conditions ranging from 0 °C to 100 °C, with added white and pink noise to account for errors due to environmental and operational conditions (EOCs) [30]. Building on the effectiveness of the CNN, Sawant et al. further developed a method for temperature-compensated damage identification and localization in GW-SHM systems using a convolutional autoencoder (TL-CAE) with a transfer learning technique to reduce the number of trainable parameters. Their unsupervised method, which does not rely on signals corresponding to damage during training, demonstrated more accurate damage detection and localization, as well as greater robustness to temperature variations, compared to supervised approaches reported on the publicly available Open Guided Waves (OGW) dataset [31]. They further extended this approach by implementing a convolutional autoencoder-based unsupervised damage detection method on an edge device [32].

Rautela et al. initially worked with temperature-affected guided waves from the OGW dataset [33], converting them into 2D representations using continuous wavelet transformation. They introduced a convolutional denoising autoencoder-based temperature compensation approach that treats the temperature effect on reference signals as noise. This denoising autoencoder was trained to transform temperature-affected signals at any temperature into signals at the reference temperature [34]. They also explored a novel physical knowledge-assisted machine learning technique, incorporating domain knowledge and expert supervision to enhance the learning process. Two supervised CNNs were trained for damage detection and localization on the same benchmark dataset under controlled temperature variations [35]. Inspired by the effectiveness of CNNs in damage detection, Rautela et al. further trained a convolutional autoencoder (CAE) exclusively on healthy signals, which were transformed into time–frequency representations using continuous wavelet transformation, to detect anomalies such as delamination in lab-controlled experiments. Anomalies were flagged when the reconstruction error exceeded a specified threshold [27]. Additionally, Rautela et al. compared deep convolutional autoencoders with other common machine learning methods for unsupervised damage detection. They combined one-dimensional support vector machines (SVM) with principal component analysis (PCA) and independent component analysis (ICA) (PCA-ocSVM and ICA-ocSVM), where PCA and ICA were used for feature extraction through linear dimensionality reduction, and SVM for relationship learning. The model was trained using baseline signals to understand their distribution and was then evaluated on new baseline and damaged signals. This evaluation focused on comparing reconstruction quality and testing accuracy across three experimental datasets: the OGW dataset [33], the NASA Prognostic Center of Excellence-Guided Waves (NASA PCoE-GW) dataset [36], and the University of Naples Computed Tomography Guided Waves (UoNCT-GW) dataset [37]. The results showed that CAE models outperformed other techniques in dynamic temperature variations, yielding superior reconstructions with reduced mean squared error and achieving higher accuracy across all datasets [23].

Apart from utilizing convolutional autoencoders, Lee et al. employed a fully connected autoencoder trained on ultrasonic signals gathered from pristine specimens. The reconstruction error was assessed using root mean square error (RMSE) to establish a statistical baseline for detecting fatigue damage, where abnormal instances were identified by significant reconstruction errors. These specimens underwent uniaxial tensile fatigue loading, with ultrasonic signals recorded periodically during the tests to study fatigue damage initiation and progression in a laboratory environment maintained at a temperature of 20 °C to mitigate temperature effects on ultrasonic signals [6]. An et al. trained an autoencoder model with ultrasonic guided waves obtained from pristine CFRP composite plates, detecting fatigue damage through the statistical baseline derived from reconstruction errors. Dominant features of the ultrasonic waves were extracted using singular value decomposition (SVD), and patterns within these features were further analyzed using unsupervised density-based spatial clustering (DBSCAN) to classify fatigue damage modes under uniaxial constant amplitude cyclic loadings [38]. Abbassi et al. also compared autoencoders with principal component analysis, kernel principal component analysis, and t-distributed stochastic neighbor embedding for unsupervised damage detection. They recommended using the residual or difference between the original sample and its reproduction from the reduced space (Q-index) and the distance to the origin in the principal component subspace (T^2-index) as damage indicators. These models were evaluated and the autoencoder also exhibited the best performance in detecting and localizing damage validated by the Open Guided Waves (OGW) dataset [33] collected from a 500 × 500 mm carbon-fiber-reinforced polymer (CFRP) plate subjected to varying temperature conditions, ranging from 20 °C to 60 °C at a constant 50% relative humidity, in controlled laboratory environments [39].

Additionally, neural network models resembling autocoders are also developed to facilitate unsupervised damage detection. For example, Zhang et al. utilized a deep convolutional neural network-based probability imaging algorithm (DCNN-PIA), resembling an autoencoder model, to automate damage detection and localization in structures [9]. In this approach, signal perturbation is introduced to the representation of normal signals to reconstruct abnormal signals for siamese network training. The damage index (DI) is derived by comparing normal state signals with testing signals in the siamese network. During training, the loss function minimizes the discrepancy between pairs of samples from the same category while maximizing it for samples from different categories. This method effectively trains the monitoring model using only signals collected under normal conditions and accurately identifies abnormal structural states. Experimental results on aluminum and composite plates demonstrate the effectiveness of the DCNN-PIA method in obtaining the DI of structures in controlled laboratory environments [9]. However, the applicability of DCNN-PIA to real-world scenarios is limited. The framework was tested only against artificially generated localized damage, while real-life structures often exhibit complex and widespread features. To address this limitation, Luca Lomazzi et al. employed convolutional autoencoders, offering a fully automatic solution applicable to real-life structures with genuine damage features. The mean squared error (MSE) between reconstructed and input signals, served as DI and was directly computed by the convolutional autoencoders, eliminating the need for additional networks. Additionally, an in-house probabilistic imaging algorithm is integrated to localize cracks in metal by corrupting the healthy baseline with noise sampled randomly from a Gaussian distribution to introduce a typical signal-to-noise ratio (SNR) value of 20 dB. The proposed method's performance was evaluated against a numerical case study involving an aluminum plate and two experimental datasets of guided waves acquired on a full-scale composite wing and a composite plate under different ambient temperatures [8].

Despite the effectiveness of autoencoder-based damage detection methods in controlled experimental setups, their performance in uncontrolled environments with irregular conditions, such as rain and snow, remains untested (**Challenge 1**). Results show that rain and snow cause significantly more variation in guided waves compared to structural damage [40]. Moreover, these reconstruction-based models typically rely on training with historical data collected under similar conditions to the test data, to reduce false alarms caused by environmental changes between training and testing [6,25,41], as illustrated in Fig. 1. This requirement poses a limitation for practical use, as it necessitates comprehensive structural health monitoring data across various environmental and operational conditions [7] (**Challenge 2**). Additionally, these methods require training data exclusively from healthy structures [7]. Our experiments have shown that if the training data includes guided waves from damaged structures, PCA and autoencoder-based models will also learn to reconstruct both normal and damage-induced guided waves, reducing their ability to detect anomalies (**Challenge 3**) [40]. To overcome these challenges, our proposed approach directly trains on current measurements, eliminating the issue of environmental and operational condition (EOC) shifts between training and testing (**Challenge 2**). This method leverages the inherent bias learning property of neural networks, where they tend to prioritize learning from more frequent classes while ignoring smaller ones [42]. As a result, the autoencoder model is more likely to learn guided waves from regular conditions, such as daily temperature and humidity changes, rather than from irregular environments like rain and snow, or damage conditions. This is because guided waves from these irregular and damaged states exhibit anomalous signals, which are underrepresented in the training data. Additionally, this method uses a local PCA reconstruction technique to help differentiate between guided waves from irregular environments and damage conditions (**Challenge 1**) [40]. Our unsupervised damage detection is based on the learning differences between reconstructing regular and damage-induced guided waves during training. Thus, the monitoring (testing) phase is integrated into the training process, removing the need for a separate test dataset, as shown in Fig. 1.

However, the third challenge still remains when the training data (current measurements) includes a significant portion of damage-induced guided waves. In such instances, the network captures more damage variations and may also learn to reconstruct these waves effectively. As a result, the reconstruction difference between healthy and damage-induced guided waves decreases, leading the autoencoder-based method to fail in detecting damage (**Challenge 3**). In this way, this work introduces a noise-augmentation strategy designed to bias the network towards learning to reconstruct healthy guided waves, rather than damage-induced ones, within the training data. Existing noise-augmentation methods in machine learning [43–45] and machine learning-based structural health monitoring (SHM) often involve adding synthetic noise — such as white Gaussian noise [8,30,31,35,45,46], impulse noise [43], triple noise [44], and pink noise [30,32] — to corrupt and expand the training data [30,31,35,46]. This enlarged dataset

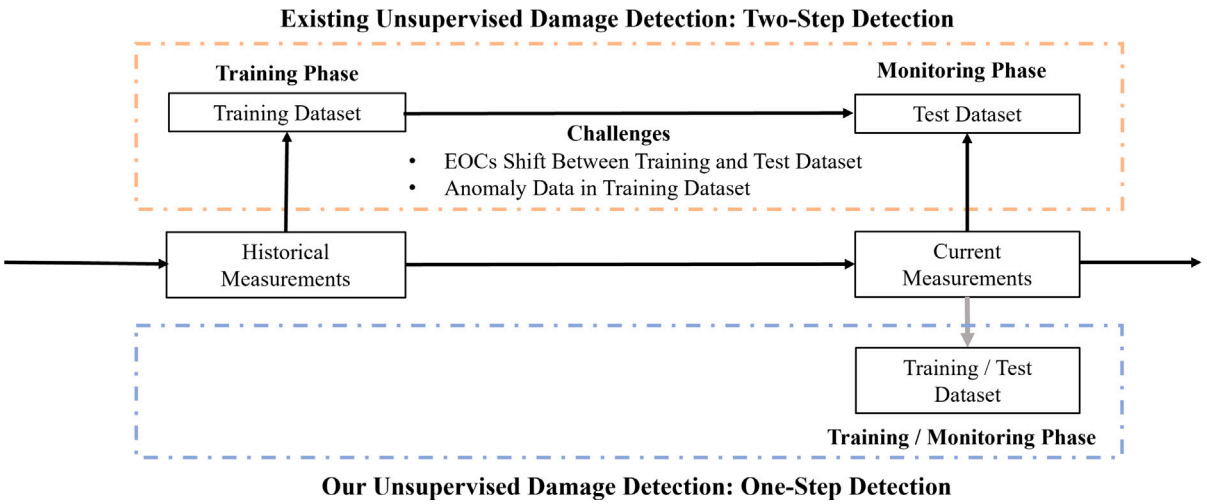

Fig. 1. Unlike existing unsupervised damage detection methods, which are trained using historical measurements, our proposed approach trains directly on current measurements. This unsupervised damage detection method performs detection in a single step during the training process, eliminating the need for an additional test dataset.

is then used to train models like convolutional neural networks [30,35,46], autoencoders [8,31], and Gaussian mixture models (GMMs) [30] to improve damage detection performance under various environmental and operational conditions. In summary, existing methods use noise augmentation to introduce a broader range of variations into the training data, aiming to reduce the environmental and operational variation shift between the training and test datasets, as illustrated in Fig. 1.

In contrast, our noise-augmentation strategy takes a different approach. We train directly on current measurements, enabling unsupervised damage detection during the training process. While traditional noise-augmentation methods aim to train models with historical measurements to recover healthy guided waves in current measurements, our approach is designed to prevent the model from learning to reconstruct damage-induced guided waves from current measurements by using noise-corrupted signals as inputs. As a result, while the optimal signal-to-noise ratio (SNR) for noise-corrupted guided waves typically ranges from 5–25 dB in existing noise augmentation research [8,30–32,35,43–46], an optimal SNR around −5 dB is more effective for damage detection in our method. It should be noted that we do not increase the size of the training dataset with our noise augmentation strategy. Instead, noise augmentation is used as a preprocessing step to adjust the noise intensity of input signals for training the recovery network.

This paper proposes two strategies to adjust noise intensity in guided waves: signal segmentation and synthetic noise addition. Firstly, guided waves exhibit varying magnitudes over time, while background noise remains relatively stable in the short term. By selecting different segments of guided waves with varying noise intensities as input to train the deep learning network to recover the entire guided waves, the learning ability to denoise damage-induced guided waves can be adjusted based on the differing noise intensities in these segments. Such a strategy is termed signal segmentation. Secondly, if the entire guided wave is relatively clean, additional noise can be incorporated into the guided waves. called synthetic noise addition technique. The learning ability to denoise damage-induced guided waves can be controlled by adjusting the intensity of additional noise. In this paper, the deep learning network used to recover entire guided waves from their segments under noisy conditions is referred to as the recovery network. By adjusting the noise intensity in guided waves, which we refer to as a noise-augmentation strategy, we can ensure that the neural network recovers healthy guided waves more accurately than damage-induced guided waves, thereby maintaining unsupervised damage detection performance even when a large proportion of damage-induced guided waves are present in training data (current measurements). The effectiveness of this unsupervised damage detection method is validated by datasets collected from uncontrolled and dynamic environmental conditions.

2. Method

In this section, this paper first introduces the unsupervised damage detection framework under complex environmental conditions. Then, the development of a recovery network incorporating a noise-augmentation strategy for enhancing damage detection is explored. Next, a brief review of the short-term PCA reconstruction method, utilized for identifying irregular environment variations, is provided. Finally, the damage detection indicators and the evaluation metric are provided at the end of the section. In this study, guided waves generated from regular environmental variations, such as daily variations in temperature and humidity, as well as those from irregular environmental variations, such as rainfall and snowfall, along with those resulting from damage, are collectively referred to as regular guided waves, irregular guided waves, and damage-induced guided waves, respectively.

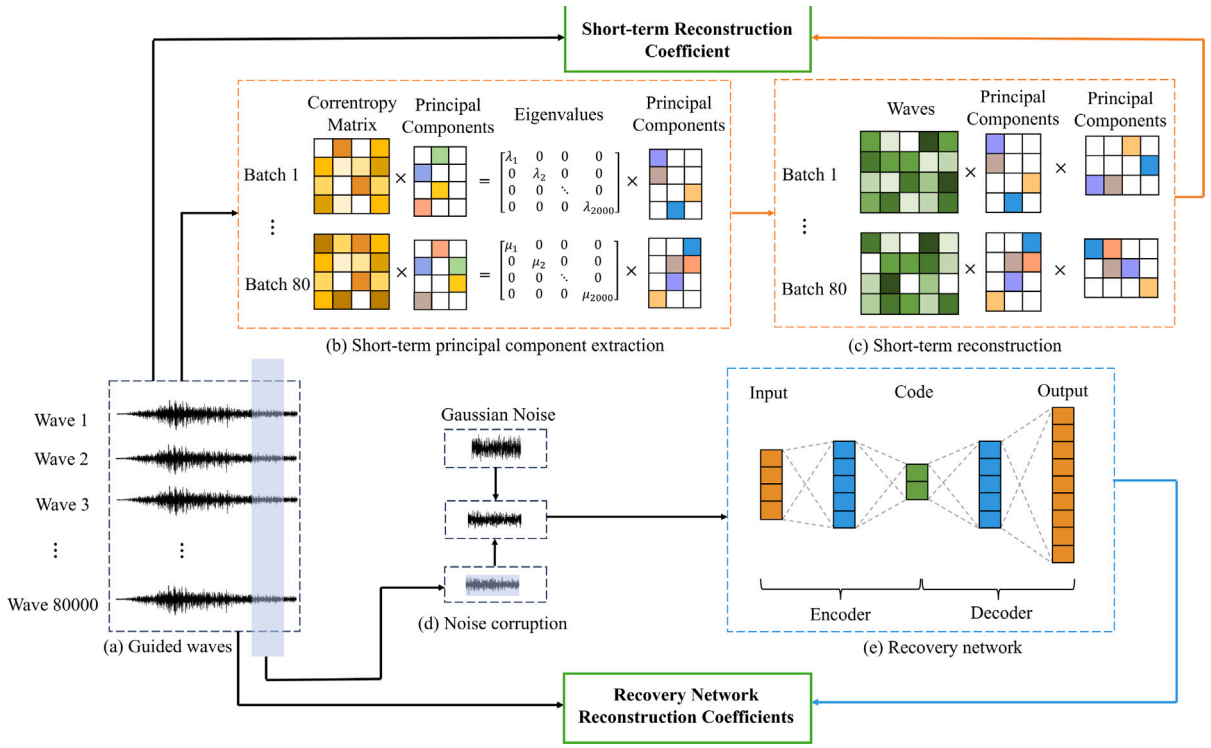

Fig. 2. The process of unsupervised damage detection is illustrated as follows: Part (a) illustrates 80-days guided waves as evaluation data. The short-term PCA reconstruction divides the 80-days evaluation dataset into 80 non-overlapping batches to extract principal components, as depicted in part (b). Subsequently, the principal components from each batch are utilized to construct a transformation matrix, which then reconstructs each batch of guided waves, demonstrated in part (c). The segments of guided waves from the evaluation data serve as the input for the recovery network, which is intentionally corrupted with additional Gaussian noise, as illustrated in part (d). The segments of guided waves (corrupted with additional noise) and the original guided waves, serving as inputs and labels, are employed to train the recovery network, shown in part (e). Reconstruction coefficients derived from the short-term PCA reconstruction (referred to as short-term PCA reconstruction coefficients) are used to identify irregular environmental variations. Meanwhile, reconstruction coefficients obtained from the recovery network, termed recovery network reconstruction coefficients, are utilized to detect variations indicative of damage.

2.1. Unsupervised damage detection framework

The unsupervised damage detection framework consists of a short-term PCA reconstruction, as illustrated in parts (b) and (c) of Fig. 2, along with a recovery network that incorporates a noise augmentation strategy, presented in parts (d) and (e) of Fig. 2. Reconstruction coefficients derived from short-term PCA, known as short-term PCA reconstruction coefficients, are employed to identify irregular environment variations. This is demonstrated in the first subplot of Fig. 3, where short-term PCA reconstruction coefficients, highlighted in blue, exhibit significant drops only during precipitation and periods of direct sunlight (indicative of temperature peaks). On the other hand, reconstruction coefficients obtained from the recovery network referred to as recovery network reconstruction coefficients, exhibit reductions in both irregular environmental variations and damage variations, as seen in the first subplot of Fig. 3, where recovery network reconstruction coefficients are marked with orange color and the damage region are shadowed by a gray region. The differences in the short-term PCA and the recovery network reconstruction to guided waves make it feasible to detect regular environmental variations, irregular environmental variations, and damage variations.

The primary distinction between the newly proposed damage detection framework and the unsupervised damage detection framework utilized in our previous research [40] is the adoption of the recovery network with a noise augmentation strategy instead of the autoencoder network. The noise intensity of inputs is managed through the utilization of signal segmentation and synthetic noise addition techniques applied to guided waves. This adjustment aims to decrease the network's capacity to recover entire damage-induced guided waves with the use of noisy inputs, thereby enhancing the framework's resilience to the presence of damage-induced guided waves within the evaluation dataset.

2.2. Reconstruction coefficient

As discussed in Section 2.1, reconstruction coefficients play a pivotal role in damage detection. These coefficients are instrumental in assessing the performance of the recovery network and the short-term PCA method in recovering and reconstructing guided waves, respectively. Specifically, they represent the Pearson correlation coefficients between the original guided waves and their recovered

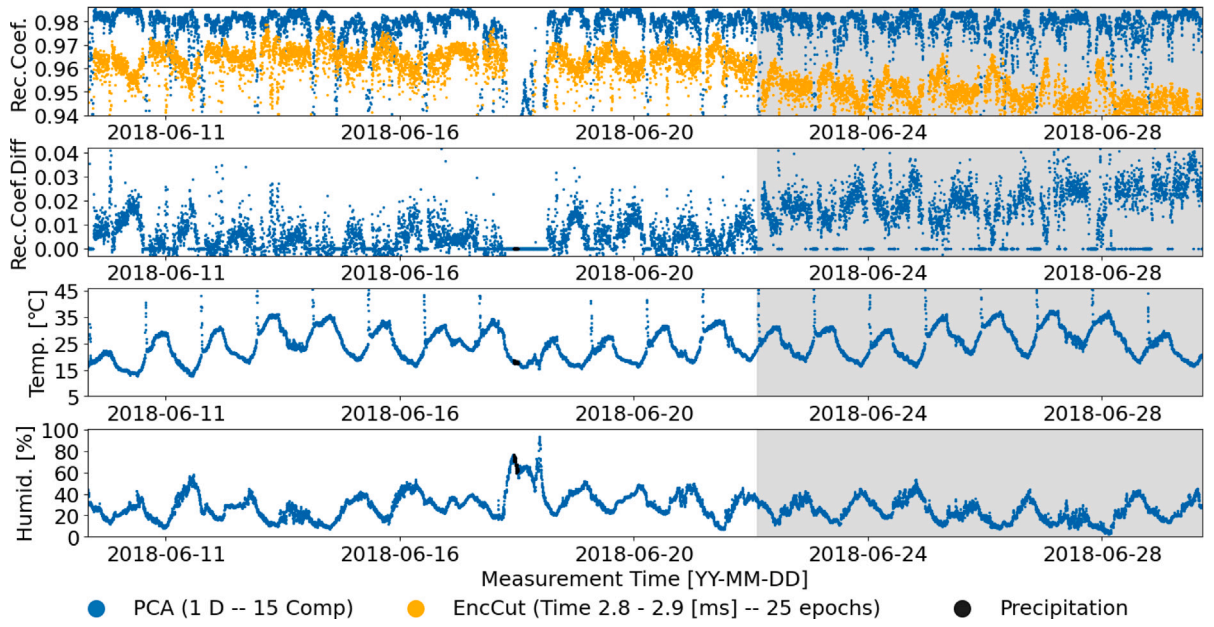

Fig. 3. The first subplot showcases the reconstruction coefficients of short-term PCA, employing a 1-day time window and the first 15 principal components, labeled "PCA (1 D – 15 Comp)", alongside recovery network reconstruction coefficients. These recovery network reconstruction coefficients are computed using the segment of guided waves from 2.8 to 2.9 ms and trained over 25 epochs, labeled "EncCut (Time 2.8–2.9 [ms] – 25 epochs)". The second subplot illustrates the normalized difference in reconstruction coefficients calculated by the two methods presented in the first subplot. Additionally, the third and fourth subplots depict the corresponding temperature and humidity for these measurements, respectively. Moments of recorded precipitation are denoted in black, while conditions of damage occurring over 8 days are shaded in gray regions. Guided wave data is sampled approximately every 86 s.

(or reconstructed) counterparts guided waves, with values ranging from −1 to 1. In this study, the evaluation dataset, denoted by $\mathbf{X}$, encompasses N guided wave measurements, each comprising M samples. This dataset is organized into a matrix format for analysis

$$\mathbf{X} = \begin{bmatrix} \mathbf{x}_1 & \mathbf{x}_2 & \dots & \mathbf{x}_N \end{bmatrix}^T , \tag{1}$$

where $\mathbf{x}_i = \begin{bmatrix} x_{i1} & x_{i2} & \dots & x_{iM} \end{bmatrix}^T$ represents a single guided wave measurement. The reconstruction coefficient is defined as

$$r_i = \frac{\left(\mathbf{x}_i' - \overline{x}_i'\right)^T \left(\mathbf{x}_i - \overline{x}_i\right)}{\|\mathbf{x}_i' - \overline{x}_i'\| \|\mathbf{x}_i - \overline{x}_i\|} \tag{2}$$

where $\|\cdot\|$ denotes the Euclidean norm. The variables $\overline{x}_i$ and $\overline{x}_i'$ represent the means of the ith guided wave measurement $\mathbf{x}_i$ and its reconstruction $\mathbf{x}_i'$, respectively.

2.3. Recovery network

The architecture of the recovery network is similar to the autoencoder network framework outlined in our prior study [40]. The recovery network also consists of both an encoder and a decoder, illustrated in part (e) of Fig. 2. In contrast to the autoencoder model that took the complete 5000 sample (or 5 ms) signal as input, the recovery network is designed to use a segment of a guided wave as the input. In this paper, we use a segment of 100 samples (or 0.1 ms). The dimensions of each layer within the encoder and decoder networks are detailed in Table 1. The recovery network is trained using the "Adam" optimizer, with a learning rate set at 0.0005 and a batch size of 256. This configuration implies that 256 guided waves are processed during each forward and backward pass of the neural network. Further specifics of the recovery network are presented in Table 1.

2.3.1. Encoder

The encoder module compresses the input vector, representing a segment of an ultrasonic guided wave ($\mathbf{x}_i \in \mathbb{R}^m$) denoted by ($\mathbf{x}_i^s \in \mathbb{R}^s$), into a low-dimensional vector of size d, where $d < s$. The activation function for neuron i in a given layer is defined as follows

$$h_i = f_{\theta}(\mathbf{x}) = \sigma\left(\mathbf{W}_e^T \mathbf{x}_e + \mathbf{b}_e\right) , \tag{3}$$

where σ denotes the tanh activation function, which is applied to produce the output h_i of a neuron within the encoder network. This output is generated following the linear transformation of $\mathbf{x}_e$, the output from the last layer, with the weight vector $\mathbf{W}_e$ and the bias vector $\mathbf{b}_e$. Consequently, the parameter set θ for the encoder comprises $\{\mathbf{W}_e, \mathbf{b}_e\}$[40,47].

Table 1
Parameters for training recovery network.

Parameters	Values in each layer
Neuron number of layers in encoder network	100 512 128 32
Neuron number of layers in decoder network	32 128 512 5,000
Learning rate	0.0005
Batch size	256

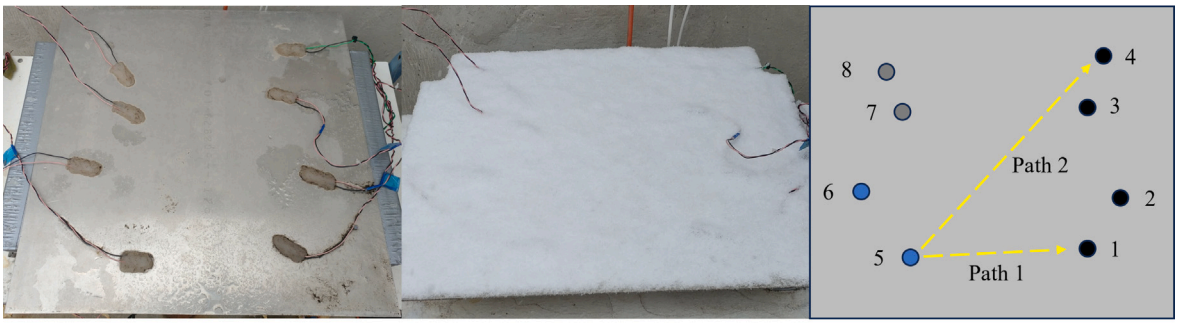

(a) Monitored Structure (Rain Weather) (b) Monitored Structure (Snow Weather) (c) Synthetic Damage Signals

Fig. 4. Parts (a) and (b), shows the monitored aluminum plate subjected to uncontrolled outdoor conditions, including various weather phenomena like rain and snow. Part (c) illustrates the locations of PZT ultrasonic sensors on the plate. Guided waves generated along Path One (the shortest path) and Path Two (the longest path) will be used to simulate damage-induced guided waves.

2.3.2. Decoder

The decoder module functions to reconstruct the ultrasonic guided wave, denoted as $\mathbf{x}_i \in \mathbb{R}^m$, from its hidden representation $\mathbf{h}_i$ (where $\mathbf{h}_i \in \mathbb{R}^d$). Accordingly, the decoder module features an increasing number of neurons across its layers. The activation function employed is given by

$$h_o = g_{\theta'}(\mathbf{x}) = \sigma\left(\mathbf{W}_d^T \mathbf{h}_i + \mathbf{b}_d\right) , \tag{4}$$

where σ is the tanh activation function. The variable θ' is the parameters $\{\mathbf{W}_d, \mathbf{b}_d\}$.

2.3.3. Loss function

We optimize the recovery network to minimize the average mean squared error between the original signals and their recovered counterparts with respect to θ and θ':

$$\begin{aligned} \theta^*, \theta'^* &= \underset{\theta,\theta'}{\operatorname{argmin}} \frac{1}{N} \sum_{i=1}^{N} \epsilon(\mathbf{x}_i, \mathbf{x}_i') \\ &= \underset{\theta,\theta'}{\operatorname{argmin}} \frac{1}{N} \sum_{i=1}^{N} \epsilon(\mathbf{x}_i, g_{\theta'}(f_\theta(\mathbf{x}_i))), \end{aligned} \tag{5}$$

where $\epsilon(\mathbf{x}_i, \mathbf{x}_i') = \sum_{j=1}^{m} (\mathbf{x}_{ij} - \mathbf{x}_{ij}')^2$ is mean square error (MSE). The objective is to make the output (recovered guided waves) as close to the original guided waves as possible.

2.3.4. Input generation and SNR estimation for signal segmentation

Instead of utilizing the entire signal, the recovery network employs segments of guided waves as inputs to train the model to recover entire guided waves. The original guided wave extends over 5 ms and consists of 5000 samples, as illustrated in the first subplot of Fig. 5. For this study, the segment size is standardized to 100 samples (lasting 0.1 ms), with the entire signal divided into non-overlapping 50 pieces. Subsequently, we assess the effectiveness of utilizing samples ranging from 0 to 0.1, 0.1 to 0.2, 0.2 to 0.3, and up to 4.9 to 5.0 ms as inputs for training the recovery network.

Guided waves exhibit varying magnitudes over time, while background noise remains relatively stable in the short term. Consequently, the noise intensity across segments at distinct guided wave positions varies. By selecting different segments of guided waves with varying noise intensities as input, the learning ability to denoise damage-induced guided waves can be adjusted. The noise intensity of each guided wave segment is quantified by the signal-to-noise ratio (SNR), which measures the ratio between the pure guided wave $\mathbf{x}_{i,s}^r$ and the background noise $\boldsymbol{\eta}$. However, the true values of the pure guided waves and background noise are unknown and thus must be estimated from the measured guided waves obtained in practical conditions. Each segment of the ith guided wave, denoted as

$$\mathbf{x}_{i,s} = \mathbf{x}_{i,s}^r + \boldsymbol{\eta} , \tag{6}$$

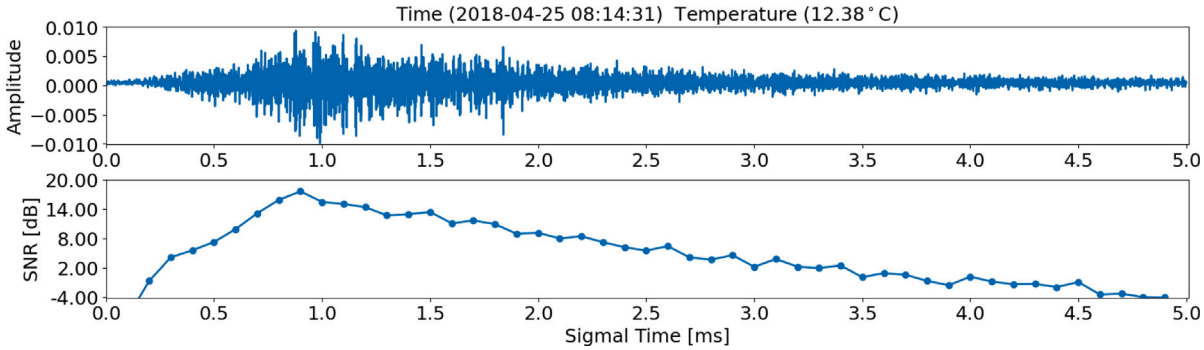

Fig. 5. The first subplot showcases a guided wave signal captured on April 25, 2018, at a temperature of $12.38°C$, denoted in the title. The second subplot visualizes the signal-to-noise ratio (SNR) for each segment of the guided wave, each segment lasting 0.1 ms and encompassing 100 samples.

which can be interpreted as the combination of the pure guided wave $\mathbf{x}^r_{i,s}$ and the background noise $\boldsymbol{\eta}$.

The noise intensity is estimated by the values of the first 50 samples (spanning from 0 to 0.05 ms) of guided waves in the evaluation data. This approach is taken because the first arrival of the guided wave to the receiver sensor occurs approximately at 70 samples (0.07 ms), indicating that signals before 0.07 ms are likely generated by background noise.

Assuming the noise is zero-mean ($E\{\boldsymbol{\eta}\} = 0$), we can estimate the noise variance $E\{\|\boldsymbol{\eta}\|^2\}$ from the first samples from 80 days (80,000 guided wave measurements) of data. Considering that the random variables $\mathbf{x}^r_{i,s}$ and $\boldsymbol{\eta}$ are statistically independent, the expectation of guided wave power can be expressed in the following:

$$E\{\|\mathbf{x}_{i,s}\|^2\} = E\{\|\mathbf{x}^r_{i,s}\|^2\} + E\{\|\boldsymbol{\eta}\|^2\} \tag{7}$$

Thus, the SNR of the sth segment of guided waves can be estimated as

$$SNR_s = 10\log_{10}\frac{P_{\text{signal}}}{P_{\text{noise}}} \tag{8}$$

$$= 10\log_{10}\frac{E\{\|\mathbf{x}_{i,s}\|^2\} - E\{\|\boldsymbol{\eta}\|^2\}}{E\{\|\boldsymbol{\eta}\|^2\}} \tag{9}$$

where each segment of guided waves comprises 100 samples. The estimated SNR of the sth segment is illustrated in the second plot of Fig. 5. It is observed that the segment of guided waves with the highest SNR is around 1 ms, corresponding to the segment with the highest amplitudes. Conversely, the magnitude of the initial and final segments of the guided waves is relatively small, resulting in very low SNR values, indicating that these segments are highly noisy. The comprehensive analysis to the SNR estimation for each segment of guided waves is provided in the appendix.

2.3.5. Synthetic noise strategy

In this paper, we demonstrate that utilizing segments of guided waves with relatively low SNR as input for the recovery network enhances damage detection performance. However, if guided waves are sufficiently clean and segments with low SNR cannot be obtained, it is rational to introduce additional noise to decrease their SNR. In this paper, Gaussian noise $\boldsymbol{\epsilon} \sim N(0, \sigma^2)$ is introduced to corrupt the guided waves. The sth segment of guided waves corrupted by Gaussian noise can be represented as:

$$\mathbf{x}^{\mathcal{N}}_{i,s} = \mathbf{x}^r_{i,s} + \boldsymbol{\eta} + \boldsymbol{\epsilon}\ , \tag{10}$$

The SNR of the sth segment of guided waves corrupted with additional Gaussian noise can be estimated as:

$$SNR^{\mathcal{N}}_s = 10\log_{10}\frac{P_{\text{signal}}}{P_{\text{noise + Gaussian noise}}} \tag{11}$$

$$= 10\log_{10}\frac{E\{\|\mathbf{x}_{i,s}\|^2\} - E\{\|\boldsymbol{\eta}\|^2\}}{E\{\|\boldsymbol{\eta}\|^2\} + E\{\|\boldsymbol{\epsilon}\|^2\}} \tag{12}$$

The entire process of deriving the SNR estimation for each segment of guided waves with additional Gaussian noise is outlined in the appendix.

2.4. Short-term PCA reconstruction

As in our previous research [40,48], short-term PCA reconstruction divides an 80-days evaluation data into nonoverlapped 80 batches of guided waves. Assuming $\mathbf{X}_t$ denote the tth batch of guided waves within $\mathbf{X}$. The dimensions of $\mathbf{X}_t$ are $L \times M$, where L encompasses the number of guided waves in each batch. In this paper, a measurement duration of 86 s, the time window size L is

set at 1000, corresponding to a duration of 1 day. $\widehat{\mathbf{X}}_t$ denotes the mean-centered version of $\mathbf{X}_t$, achieved by subtracting the mean of each column from $\mathbf{X}_t$. The short-term PCA reconstruction process is shown in part (b) and (c) of Fig. 2.

In short-term PCA reconstruction, the principal components utilized for reconstructing guided waves are the eigenvectors of the correlation matrix for samples of guided waves. The estimated covariance matrix $\mathbf{C}$ for samples of guided waves batch $\mathbf{X}_t$ is given by

$$\mathbf{C} = \widehat{\mathbf{X}}_\mathbf{t}^T \widehat{\mathbf{X}}_\mathbf{t} \tag{13}$$

Then eigenvalue decomposition is carried out on the estimated covariance matrix to derive the eigenvalues and their associated eigenvectors.

$$\mathbf{C}v_i = \lambda_i v_i \tag{14}$$

where v_i is a vector of length M and λ_i is the corresponding eigenvalue.

Reconstruction of guided waves is realized through the transformation matrix $\mathbf{V}$, having dimensions $M \times P$. This matrix incorporates the first P principal components, which correspond to the P largest eigenvalues of the correlation matrix $\mathbf{C}$. The transformed representation, denoted as $\mathbf{Y}$ with a dimension of $L \times P$, is calculated as follows:

$$\mathbf{Y} = \widehat{\mathbf{X}}\mathbf{V} \tag{15}$$

The guided wave reconstruction is achieved by

$$\widehat{\mathbf{X}}' = \mathbf{Y}\mathbf{V}^\mathbf{T} \tag{16}$$

The reconstructed guided waves batch $\mathbf{X}'_t$ is then obtained by adding each column mean of $\mathbf{X}_t$ back into $\widehat{\mathbf{X}}'_t$.

2.5. Irregular and damage variation detection

The short-term PCA reconstruction coefficients are designed to identify irregular environmental variations, such as rain and snow, according to

$$\mathbf{r}_\mathbf{i}^{(S)} \leq \lambda. \tag{17}$$

As shown in the first subplot of Fig. 3, the short-term reconstruction coefficients, highlighted in blue, exhibit a decrease particularly during irregular environmental variations, such as precipitation events denoted in black. Consequently, irregular environmental variations are identified when short-term reconstruction coefficients fall below a threshold denoted by λ. In this context, λ is defined as the 20-th percentile of short-term reconstruction coefficients obtained from the evaluation data. This choice is made under the consideration that irregular environmental variations represent a relatively small portion of the evaluation data [48,49].

Damage variations are identified by contrasting short-term PCA and recovery network reconstruction coefficients. As depicted in the first subplot of Fig. 3, while recovery network reconstruction coefficients decline within damage regions highlighted in gray, short-term PCA reconstruction coefficients remain unaffected. Thus, the disparity between short-term PCA and recovery network reconstructions can serve to detect damage variations. To alleviate reconstruction differences stemming from regular environmental variations, we normalize short-term and recovery network reconstruction coefficients using their respective medians $r^{(S)}_{\text{median}}$ and $r^{(L)}_{\text{median}}$ across the entire evaluation dataset. Consequently, the normalized discrepancy between short-term PCA and recovery network reconstruction coefficients is considered as damage indicators, defined as

$$\Delta = \frac{r_i^{(S)}}{r_{median}^{(S)}} - \frac{r_i^{(L)}}{r_{median}^{(L)}} \tag{18}$$

In this context, $r_i^{(S)}$ and $r_i^{(L)}$ represent the short-term PCA and recovery network reconstruction coefficients for the ith guided wave, respectively. When the discrepancy Δ exceeds the threshold η, it indicates the occurrence of damage variations. However, the specific value of η is not explicitly defined in this study. Instead, we utilize the receiver operating characteristic (ROC) curve to evaluate the performance of the recovery network reconstruction method for damage detection, a widely adopted technique in structural health monitoring [50].

It is crucial to emphasize that the normalized reconstruction difference significantly increases during irregular environment variations. To mitigate this effect, we reset the normalized reconstruction difference to 0 for measurements that potentially satisfy the criteria defined in (17), guided by their corresponding short-term reconstruction coefficients. These recalibrated normalized reconstruction differences are subsequently utilized as the metric for damage detection [40,48].

2.6. Damage detection evaluation

In this study, we evaluate performance using the area under the curve (AUC) of the receiver operating characteristic (ROC) curve. This approach facilitates a thorough assessment across all potential values of η, negating the need for defining a particular threshold. Within the ROC curve, the x-axis corresponds to the false positive rate (FPR), while the y-axis represents the true positive rate (TPR).

3. Experiment

We assess the efficacy of the noise-augmentation strategy in enhancing the robustness of the recovery network to the presence of damage-induced guided waves in the evaluation data, utilizing the same dataset employed in the autoencoder reconstruction-based damage detection study [40]. Our evaluation dataset consists of ultrasonic guided waves acquired from an aluminum plate measuring 53 cm by 53 cm by 3 mm, situated at the University of Utah in Salt Lake City. This plate is situated on the top shelf within a small, three-walled room equipped with a gate but lacking a roof, thereby exposing the structure and monitoring system to dynamic outdoor conditions, including various weather phenomena such as rain and snow. In the monitoring setup, each measurement entails capturing 8 ultrasonic guided waves, alongside environmental parameters such as temperature, humidity, air pressure, and brightness. Further details regarding the measurement collection procedure are depicted in previous literature [49,51].

3.1. Synthetic damage guided wave generation

The dataset used to train the model and evaluate the effectiveness of our method consists of guided waves collected from Path 5–1, as shown in part(c) of Fig. 4. It also includes guided waves with synthetic damage information, created using a method similar to those employed in previous studies [50]. According to this technique, a guided wave with damage variations is interpreted as the result of combining a direct guided wave from the transmitter and another guided wave that has interacted with a damage site [50,52,53], as illustrated in part (b) of Fig. 4. Consequently, guided waves representing damage variations are synthesized by leveraging guided waves from both the shortest (path one) and longest signal path (path two), as illustrated in previous work [48].

$$\widehat{\mathbf{x}}_i = \mathbf{x}_i^{(B)} + \gamma \mathbf{x}_i^{(D)} , \tag{19}$$

where $\mathbf{x}_i^{(B)}$ is the ith guided wave from the shortest path (path one) and $\mathbf{x}_i^{(D)}$ is the ith guided wave from the longest path (path two). The variable γ is the scattering factor and is set to 0.2, which follows prior literature [48]. It is important to note that signals with synthetic damage are derived from guided waves collected simultaneously along two different paths. However, we use guided waves affected by various environmental and operational conditions, such as rain and snow, to simulate guided waves with damage information under different scenarios, as shown in parts (a) and (b) of Fig. 4.

3.2. Training, test, and validation dataset

Since our method achieves unsupervised damage detection (monitoring phase) during the training process (training phase), as illustrated in Fig. 1, the training data also serves as the test data, eliminating the need for additional test data. Additionally, our method does not require a validation dataset, which is commonly used in supervised learning to prevent overfitting [54]. Instead, our approach involves overfitting the recovery network to reconstruct regular guided waves from the training data. To construct train/test data, we create 10 regions of guided waves from the entire measurement dataset. Each region comprises 80,000 guided wave measurements (approximately 80 days) collected from sensor path 5-1, as shown in Fig. 4. Each measurement includes 5000 guided wave samples (lasting 5 ms). Synthetic damage is introduced towards the end of each region, varying from 2 to 20 days.

4. Results and discussion

This section demonstrates how the noise-augmentation strategy improves the unsupervised damage detection performance when the training data contains a large ratio of damage-induced guided waves. The improvement is evaluated using the AUC score, computed from the normalized discrepancy between short-term PCA reconstruction coefficients and recovery network reconstruction coefficients. Initially, we investigate the variation in AUC scores with segments of guided waves exhibiting different natural noise intensities. Subsequently, we explore the change in AUC scores with segments of guided waves corrupted with different levels of additional noise, validating the impact of augmented noise on damage detection performance. Finally, guidelines for selecting an appropriate noise intensity to enhance the robustness of unsupervised damage detection will be provided at the end of this section.

4.1. Effects of natural noise in guided waves on damage detection

Fig. 6 presents the recovery network reconstruction coefficients obtained from segments of samples spanning different time intervals: 0.1 to 0.2 ms, 1.2 to 1.3 ms, 3.0 to 3.1 ms, and 4.9 to 5.0 ms. Notably, when utilizing segments at the starting positions of guided waves as input for training the recovery network, such as the segment from 0.1 to 0.2 ms, as depicted in the first subplot of Fig. 6, the reconstruction coefficients achieved after 10, 20, and 30 epochs of training are only around 0.6. This indicates significant deviation between the recovered guided waves by the network and the original guided waves. Furthermore, it is crucial to note the absence of observable reconstruction discrepancy between regular guided waves and damage-induced guided waves, as evidenced by the shaded gray regions in Fig. 6. This lack of differentiation arises because the segment at the starting positions of guided waves is inherently noisy (for instance, the natural SNR of the segment from 0.1 to 0.2 ms is approximately −8.1 dB, as shown in Fig. 6) due to the small magnitude of excited signals, as illustrated in the first subplot of Fig. 5. Consequently, the input contains minimal information about the overall guided waves, making it challenging for the network to be adequately trained to accurately recover the entire guided waves. As a result, damage detection based on reconstruction differences between regular guided waves and damage-induced guided waves cannot be effectively achieved.

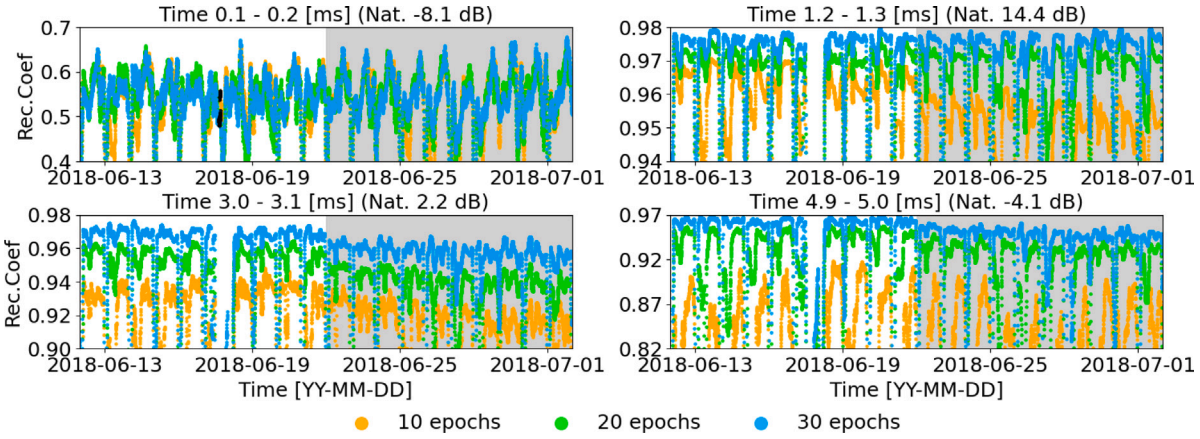

Fig. 6. The four subplots illustrate the reconstruction coefficients generated by a recovery network using the signal segmentation strategy. Each subplot displays reconstruction coefficients using segments of guided waves as inputs from: 0.1 to 0.2 ms, 1.2 to 1.3 ms, 3.0 to 3.1 ms, and 4.9 to 5.9 ms, respectively, as labeled in their titles. Additionally, the estimated natural SNR of each segment of guided waves (−8.1 dB, 14.4 dB, 2.2 dB, and −4.1 dB) is provided in the title of each subplot. Within each subplot, reconstruction coefficients from 10, 20, and 30 epochs are depicted in orange, green, and blue, respectively. The damage region persists for 10 days and is shaded in gray color.

When utilizing a segment of guided waves with a high SNR as inputs to train the recovery network, such as the segment from 1.2 to 1.3 ms with a natural SNR of approximately 14.4 dB, the resulting reconstruction coefficients after 10, 20, and 30 training epochs are notably high, around 1, as shown in the second subplot of Fig. 6. This indicates that this segment of guided waves can effectively recover the entire guided waves. This is facilitated by the significantly higher magnitude of this segment of guided waves, as illustrated in the first subplot of Fig. 5, enabling it to contain ample information pertinent to the entire guided waves. Moreover, it is noteworthy that we can discern reconstruction disparities between regular guided waves and damage-induced guided waves after 10 training epochs. However, with continued training epochs, such as 20 and 30 epochs, the reconstruction coefficients for damage-induced guided waves tend to overfit to the measurement with damage. Consequently, damage detection based on the reconstruction differences among these guided waves becomes challenging in this scenario.

When utilizing more noisy segments of guided waves as input to train the recovery network, such as the segment from 3.0 to 3.1 ms with a natural SNR of 2.2 dB or from 4.9 to 5.0 ms with a natural SNR of −4.1 dB, as depicted in Fig. 5, the reconstruction disparities for regular and damage-induced guided waves persist even after 30 training epochs. This is seen in the third and fourth subplots of Fig. 6. This suggests that using segments of guided waves with relatively strong noise intensity as inputs make the recovery network less effective at learning to recover damage-induced guided waves compared to regular guided waves even when a large ratio of damage-induced guided waves exists in training data.

Fig. 7 presents AUC scores for different natural noise conditions as a function of damage duration and number of training epochs. In first top-left subplot shows the original autoencoder-based damage detection AUC scores, where the input comprises of entire guided wave signals. The subsequent subplots depict recovery network-based damage detection, where inputs consist of segments of guided waves with varying noise intensity. It is noticeable that selecting segments of guided waves with very high noise levels as inputs, such as the segment from 0.1 to 0.2 ms, yields lower AUC scores across different training epochs and varying damage durations in the training data when compared to those obtained with the original autoencoder. Choosing segments of guided waves with low noise intensities as the input, such as the segment from 1.2 to 1.3 ms, results in rapidly decreasing AUC scores with increasing training epochs or longer damage durations because the recovery network is overfitting to the damage-induced guided waves. In contrast, high AUC scores can be maintained for a large number of training epochs and a large ratio of damage-induced guided waves when segments of guided waves have a suitable noise intensity, such as the segment from 2.8 to 2.9 ms.

Fig. 8 shows the change in the average AUC scores over training epochs with different segments of guided waves as inputs and damage durations, as denoted in the title of each subplot. Each subplot also includes the estimated natural SNR and average reconstruction coefficients over all regular and damage-induced guided waves, labeled as “Avg. Normal RC” and “Avg. Abnormal RC”, respectively, for the segments of guided waves used. The natural SNR of each segment of guided waves is normalized to a range of 0.6 to 1, labeled as “Norm. SNR” to facilitate a comparison of the AUC scores and the average reconstruction coefficients for regular (“Normal RC”) and damage-induced (“Anomaly RC”) guided waves. Fig. 8 illustrates that the normalized SNR exhibits an initial increase followed by a decrease. The AUC scores with excessively low or high SNRs are lower compared to those with suitable SNRs. Using segments with suitable noise intensity, such as those from the later part of guided waves, have AUC scores are significantly higher than the average AUC scores calculated with the autoencoder reconstruction, labeled “Avg. AUC (Enc)”. Consequently, optimizing the noise intensity in segments of guided waves as input can enhance both the robustness and peak performance, even in scenarios where a significant proportion of damage-induced guided waves exists in the training data.

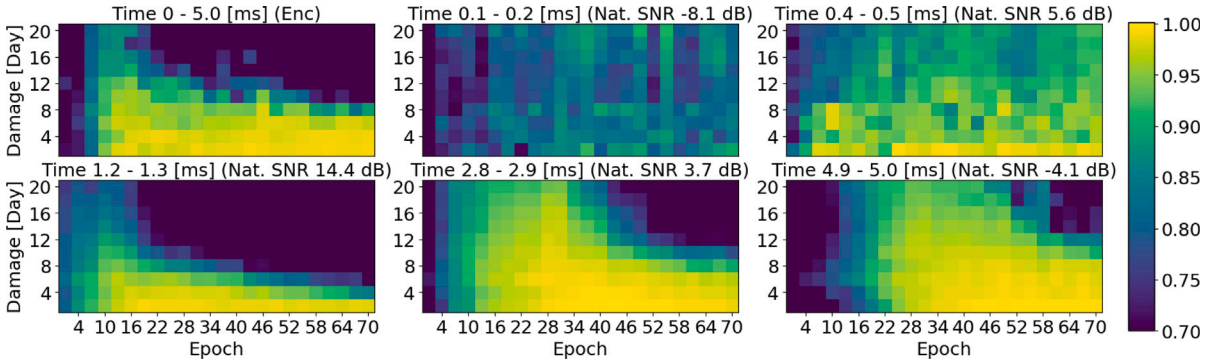

Fig. 7. The six subplots illustrate the change of the AUC score with training epochs (x-axis) ranging from 1 to 70 epochs, and damage duration (y-axis) ranging from 2 to 20 days. The first subplot showcases AUC scores calculated with the original autoencoder, labeled as "Time 0–5.0 [ms] (Enc)". The subsequent five subplots display results from the recovery network with segments of guided waves from, 0.1 to 0.2 ms, 0.4 to 0.5 ms, 1.2 to 1.3 ms, 2.8 to 2.9 ms, and 4.9 to 5.0 ms, respectively, each labeled accordingly in their titles. Additionally, the estimated natural SNR of each segment of guided waves (−8.1 dB, 5.6 dB, 14.4 dB, −3.7 dB, and −4.1 dB) is provided in the title of each subplot. The color bar denotes the range of AUC scores.

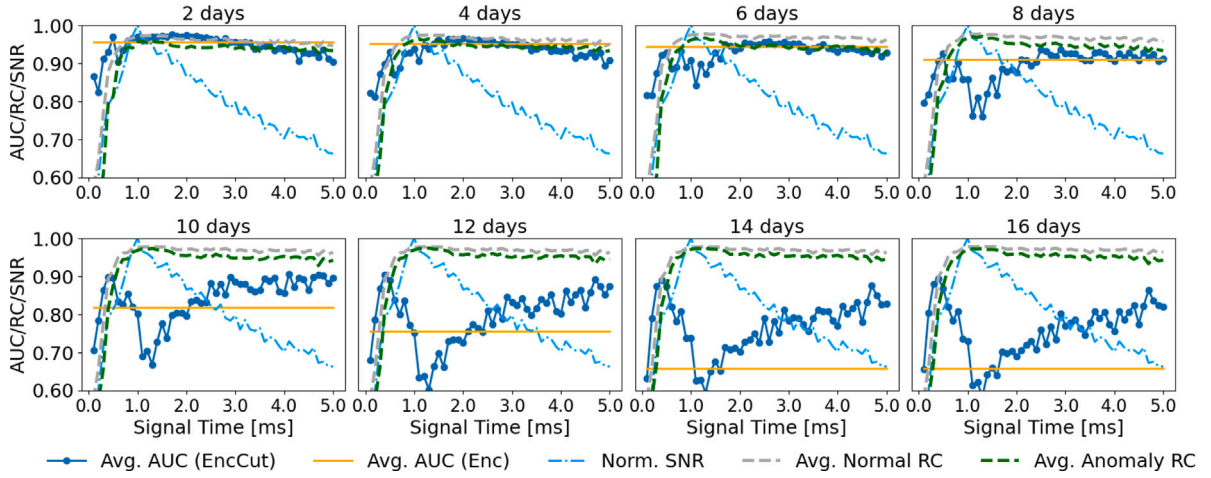

Fig. 8. Each subplot illustrates the change of the average of AUC scores over training epochs, the average of reconstruction coefficients over 80-days measurements, and normalized SNR values, (labeled with "AUC/RC/SNR" in the y-axis) with each segment of guided waves utilized in training the recovery network (labeled "Measurement Time [ms]"in the x-axis) when the damage persists from 2 to 16 days, designated in the title of each subplot. Notably, in each subplot, the average AUC score computed with the recovery network using the signal segmentation strategy is highlighted in blue. Each guided wave segment lasts 0.1 ms and spans from 0 to 0.1 ms, 0.1 ms to 0.2 ms, up to 4.9 to 5.0 ms. Additionally, the average AUC score calculated with the original autoencoder reconstruction coefficients is depicted (marked with orange color) as the reference to demonstrate the improvement achieved by the signal segmentation strategy. The average reconstruction coefficients from regular and damage-induced guided waves are presented and labeled with gray and green colors, respectively.

4.2. The effect of synthetic noise intensity in guided waves on damage detection

Fig. 8 highlights the impact of the natural noise on the performance of damage detection. The lowest average AUC score over training epochs is evident when utilizing the segment around 1.2 to 1.3 ms, exhibiting the highest SNR among these guided wave segments. It should be noted that identical time segments of guided waves collected at different times will have varying SNRs due to environmental changes that affect wave propagation. To improve the damage detection performance using segments with high natural SNR and further verify that the SNR of guided wave segments influences the performance of reconstruction-based anomaly detection, we add white Gaussian noise to the identical segment of each guided wave to create input signals with the same noise intensity (SNR) before using it to train the recovery network. Fig. 9 illustrates the effects of this additional noise. The first subplot in Fig. 9 shows reconstruction coefficients without additional noise. Upon adding Gaussian noise to adjust the SNR of the segment to approximately 8.1 dB, the reconstruction coefficients experience a slight decrease, but the patterns remain similar. As more noise is added to the segment of guided waves to reduce their SNR to −0.4 dB, the network no longer adequately recovers damage-induced guided waves, allowing us to distinguish them from regular guided waves. As when we continue decrease the SNE to −4.8 dB, the results become too noisy to adequately separate the two scenarios. Fig. 10 illustrates the change in AUC scores with training epochs and damage duration in the training data for the segment of guided waves from 1.2 to 1.3 ms. As more noise is added to reduce the

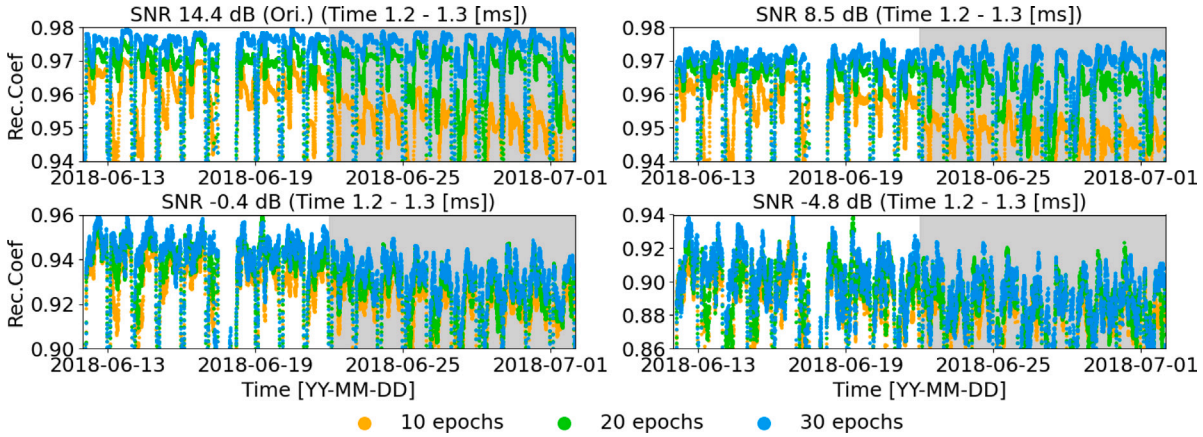

Fig. 9. The four subplots depict reconstruction coefficients computed using the segment of guided waves from 1.2 to 1.3 ms after training the recovery network for 10, 20, and 30 epochs, respectively. In the first subplot, reconstruction coefficients are derived from original guided waves with a SNR of 14.4 dB. In the subsequent subplots, reconstruction coefficients are derived from guided waves corrupted by additional noise to achieve SNRs of 8.5 dB, −0.4 dB, and −4.8 dB (as labeled in the title of each subplot), respectively. Damage regions persist for 10 days and are shaded in gray.

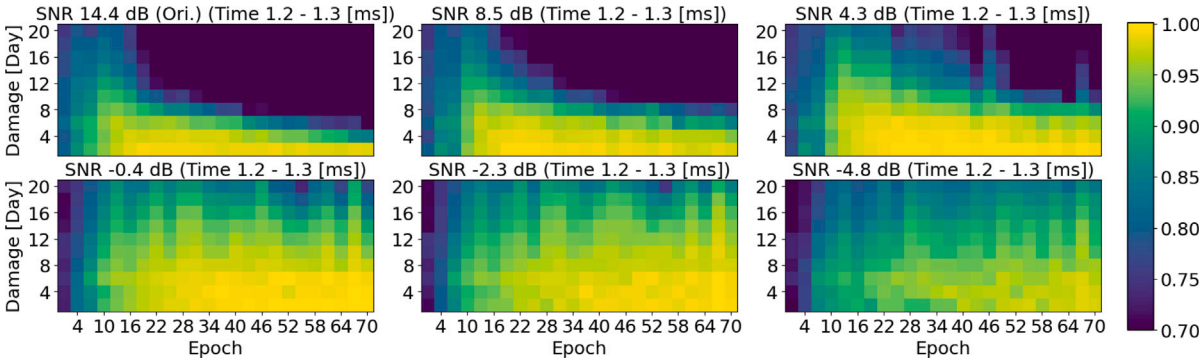

Fig. 10. The six subplots illustrate the change of the AUC score with training epochs (x-axis) ranging from 1 to 70 epochs, and damage duration (y-axis) ranging from 2 to 20 days. The first subplot presents AUC scores computed using the segment (ranging from 1.2 to 1.3 ms) of the original guided waves with a SNR of 14.4 dB. The subsequent five subplots display AUC scores calculated with the segment (ranging from 1.2 to 1.3 ms) of guided waves corrupted by additional noise to achieve SNRs of 8.5 dB, 4.3 dB, −0.4 dB, −2.3 dB, and −4.8 dB, labeled accordingly in the title of each subplot.

SNR of the segment to 8.5 dB, 4.3 dB, and −0.4 dB, higher AUC scores are achieved for larger training epochs with larger damage durations. However, with more noise, the AUC scores gradually decrease due to poor guided wave reconstruction.

Fig. 11 illustrates the change in the average AUC scores over training epochs, labeled "Avg. AUC (EncCut)", using the guided wave segment ranging from 1.2 to 1.3 ms with varying additional noise intensity ranging from −15 to 10 dB. The average reconstruction coefficients for regular and damage-induced guided waves, labeled as "Avg. Normal RC" and "Avg. Abnormal RC", are also provided. We observe that as additional noise increases, the average reconstruction coefficients for regular guided waves and damage-induced guided waves gradually decrease but the difference between the two average reconstruction coefficients increases, leading to an increase in the AUC scores over training epochs. As more noise is added, the AUC scores begin to decrease while the average reconstruction coefficients decrease rapidly. This indicates that the recovery network struggles to recover the guided wave signals, thereby worsening damage detection due to an increase in false alarms. Compared with the AUC scores calculated with the original autoencoder, which takes the entire guided waves as input and is labeled as "Avg. AUC (Enc)", adding suitable Gaussian noise significantly improves damage detection performance. Additional evidence is presented in Figs. 12 and 13, where the guided wave segments (input signals for the recovery network) range from 4.0 to 4.1 ms and 4.9 to 5.0 ms, respectively.

Besides white Gaussian noise, we also used white Laplace noise, white Cauchy noise, and pink noise to corrupt guided wave segments. We then used these noise-corrupted segments as inputs to recover the original guided waves and calculated the corresponding AUC scores based on the recovery network's reconstruction coefficients. Fig. 14 illustrates the change in average AUC scores over training epochs for the segment (ranging from 1.2 to 1.3 ms) of guided waves corrupted with additional noise, achieving SNRs from −15 to 10 dB. In each subplot of Fig. 14, the average AUC scores for guided waves corrupted with white Gaussian noise, white Laplace noise, and white Cauchy noise — labeled "Gaussian", "Laplace", and "Cauchy", respectively — are quite similar. In contrast, the average AUC score for guided waves corrupted with pink noise, labeled in light blue, required a lower SNR (stronger noise intensity) to achieve a similar AUC score compared to the white noise types. This difference may be due

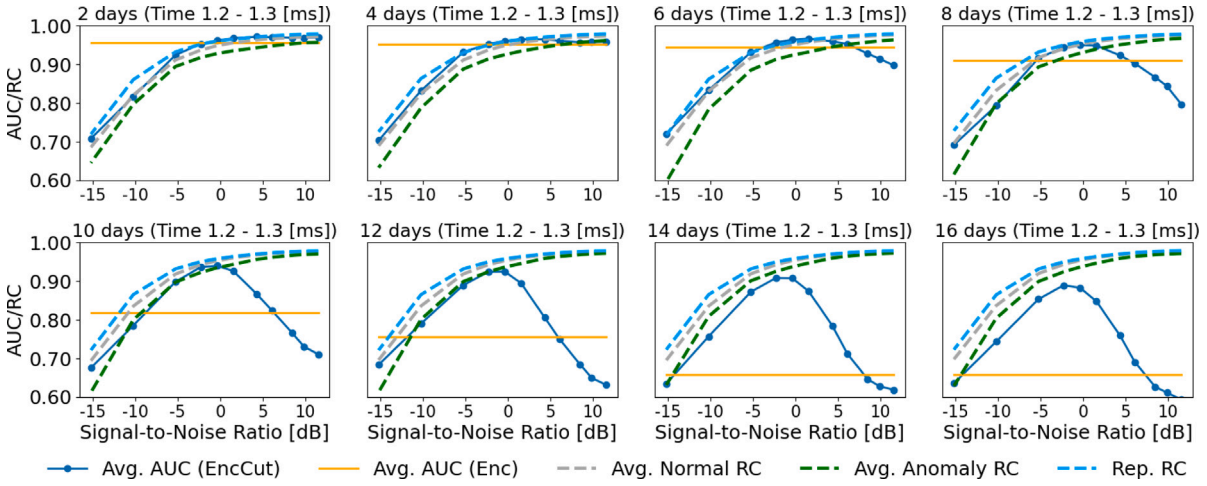

Fig. 11. Each subplot illustrates the variation of the average AUC scores over training epochs and the average of reconstruction coefficients over 80-days measurements (labeled "AUC/RC" in the y-axis) using the segment (ranging from 1.2 to 1.3 ms) from guided waves corrupted with additional noise to achieve SNRs from −15 to 10 dB (labeled "Signal-to-Noise Ratio" in the x-axis), while the damage persists from 2 to 16 days, as designated in the title of each subplot. In each subplot, the average AUC score computed with the recovery network using the segment of guided waves as inputs is highlighted in blue. Additionally, the average AUC score calculated with the autoencoder reconstruction coefficients is depicted (marked with orange color) to showcase the improvement achieved by the additional noise to guided waves. The average reconstruction coefficients from regular and damage-induced guided waves, along with the median of all reconstruction coefficients, are presented in light blue, green, and gray colors, respectively, and labeled as "Avg. Normal RC", "Avg. Abnormal RC", and "Rep. RC".

to pink noise having a specific frequency pattern, making it more structured and predictable than uncorrelated noises like white noise. Consequently, using pink noise necessitates a higher noise intensity (lower SNR) to achieve the same effect of preventing the recovery network from reconstructing damage-induced guided waves. Overall, the four types of noise significantly improve damage detection compared to the autoencoder-based damage detection, labeled "Enc" in Fig. 14.

4.3. Explanation for noise augmentation to the unsupervised damage detection with t-SNE

Fig. 15 illustrates the distribution of the recovery network's latent space in a two-dimensional t-SNE plot as the SNR of the input signals (the segment of guided waves) varies from 14.5 dB to −15.2 dB. It shows that the distribution of irregular guided waves, marked in orange, differs significantly from that of regular and damage-induced guided waves. Conversely, the distributions of regular and irregular guided waves are very similar when the noise intensity is not extremely high, such as with an SNR smaller than −5 dB, as depicted in Fig. 15. This explains why the recovery network can reconstruct regular and damage-induced guided waves more effectively than irregular guided waves since it primarily learns to the distribution of dominant variations (regular and damage variations). However, when the SNR drops to very low levels, such as below −10 dB, no clear distribution patterns for regular, irregular, and damage-induced guided waves are evident, as shown in the last two subplots of Fig. 15. In these cases, the recovery network struggles to learn to distribution patterns of guided waves under such noisy conditions, leading to poor reconstruction. On the other hand, when the noise intensity of the input signals reduces to suitable levels like 4 dB, as shown in the fourth subplot of Fig. 15, the distribution of regular and damage-induced guided waves becomes more distinct, even though it becomes fuzzy. This increased separation enhances the reconstruction differences between regular and damage-induced guided waves, thereby improving damage detection and increasing the AUC score, as indicated in the titles of the subplots in Fig. 15.

4.4. Guidelines for noise augmentation to the unsupervised damage detection

The results suggest that the noise intensity of input signals (segments of guided waves) is crucial to improve the unsupervised damage detection framework when the training data contains a large ratio of damage-induced guided waves. The noise intensity can be optimized by selecting segments of guided waves with suitable noise intensity (SNR) and/or incorporating additional noise into segments of guided waves. Consequently, a critical question arises regarding the estimation of suitable noise intensity of inputs to improve the damage detection performance.

Fig. 11 indicates that adding either very light or very heavy noise to the guided wave segments does not enhance damage detection performance. Instead, achieving an SNR close to −3 dB yields the best results. Further evidence is provided by Fig. 12, where the segment of guided waves ranging from 4.0 to 4.1 ms yields peak average AUC scores when Gaussian noise is added to achieve an SNR also close to −3 dB. Similarly, Fig. 13 reveals that for the segment of guided waves ranging from 4.9 to 5.0 ms, whose natural SNR is already close to −3 dB, the addition of a small amount of Gaussian noise results in an immediate decrease in the average AUC score. These findings indicate that the segment of guided waves with an SNR of −3 dB is suitable for this dataset.

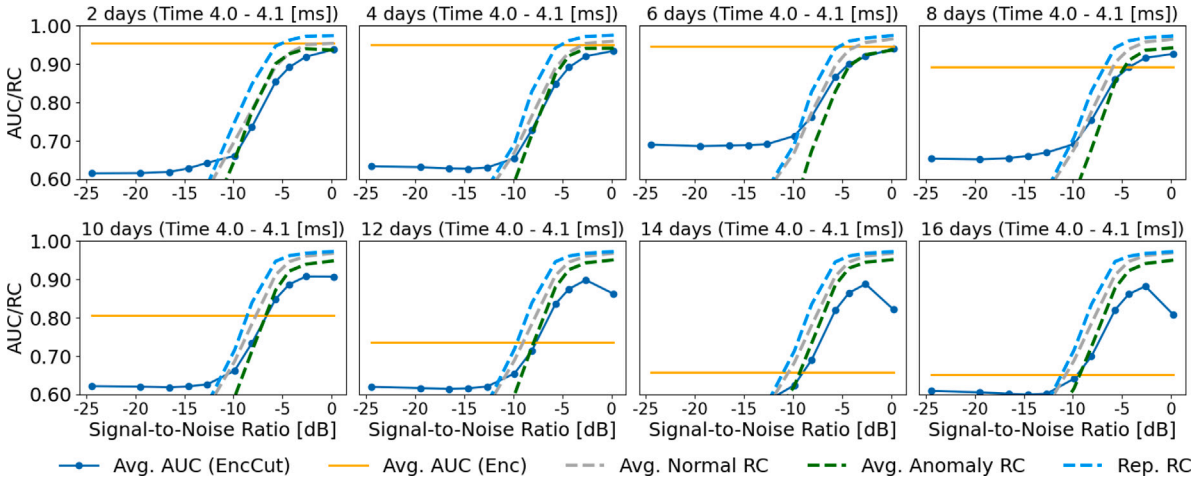

Fig. 12. The results depicted in each subplot resemble those presented in Fig. 11. However, in these subplots, the average AUC score over the training epoch is calculated with the segment (ranging from 4.0 to 4.1 ms) from guided waves.

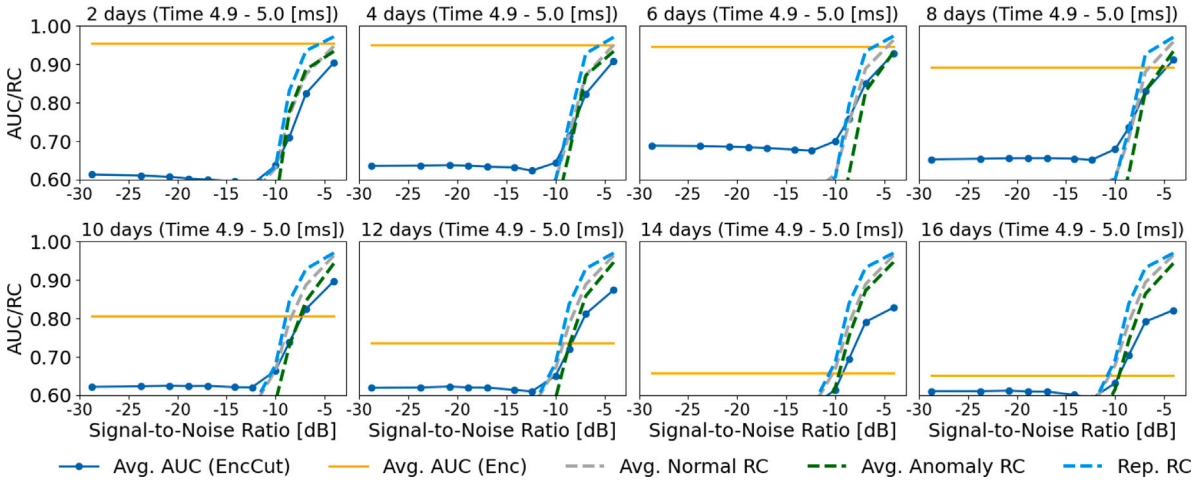

Fig. 13. The results depicted in each subplot resemble those presented in Fig. 11. However, in these subplots, the average AUC score over the training epoch is calculated with the segment (ranging from 4.9 to 5.0 ms) from guided waves.

It is important to note that −3 dB may not be an appropriate noise intensity for input signals collected under other conditions. However, we observe from Figs. 11 to 13 that an increase in AUC scores correlates with a rise in the representative reconstruction coefficient (labeled "Rep. RC"), defined as the median of the reconstruction coefficients across the guided waves. The optimal noise intensity is reached shortly after the representative reconstruction coefficient begins to stabilize. By monitoring these representative reconstruction coefficients, we can identify the optimal noise intensity to maintain effective unsupervised damage detection performance without relying on any damage label information for evaluation.

5. Conclusions

This paper introduces a neural network designed to recover entire guided waves from segments of guided waves (recovery network), enabling unsupervised damage detection solely trained with the current measurements. To enhance the performance of this unsupervised damage detection method when training data contains a significant proportion of damage-induced guided waves, a noise-augmentation technique is proposed to modulate the network's learning capacity to recover damage-induced guided waves by controlling the noise intensity of input signals.

Two noise-augmentation strategies are proposed to adjust the noise intensity of input signals for the recovery network. The first strategy, known as signal segmentation, involves dividing guided waves into segments at various positions since the amplitudes of guided waves vary over time, leading to variations in SNR. The second strategy, synthetic noise addition, incorporates additional

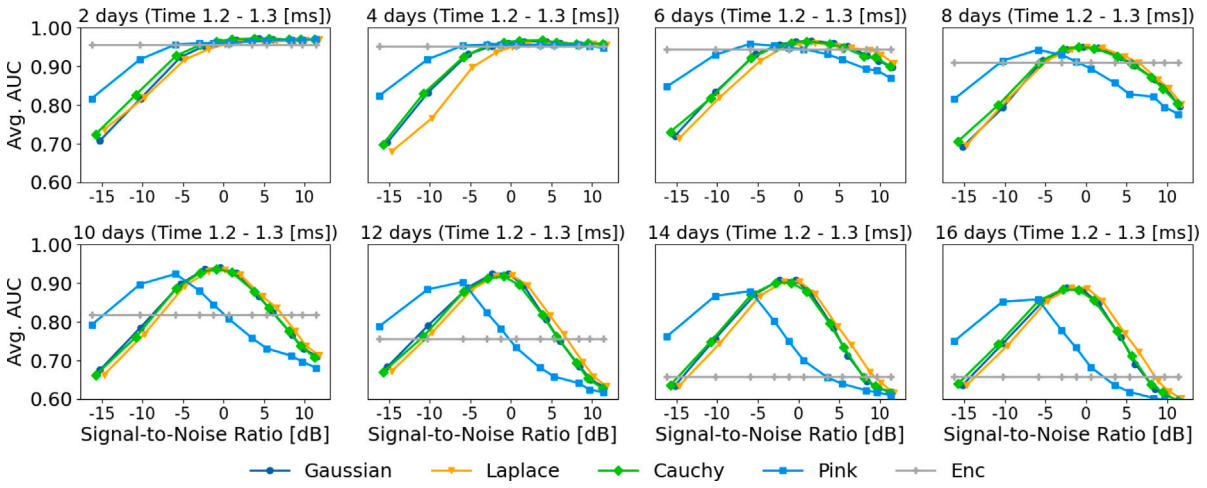

Fig. 14. Each subplot illustrates the variation of the average AUC scores over training epochs using the segment (ranging from 1.2 to 1.3 ms) from guided waves corrupted with additional noise to achieve SNRs from −15 to 10 dB (labeled "Signal-to-Noise Ratio" on the x-axis), while the damage persists from 2 to 16 days, as designated in the title of each subplot. In each subplot, the average AUC scores for guided waves corrupted with white Gaussian noise, white Laplace noise, white Cauchy noise, and pink noise are labeled "Gaussian", "Laplace", "Cauchy", and "pink", respectively. The average AUC score over training epochs for the autoencoder using the original guided waves is labeled "Enc".

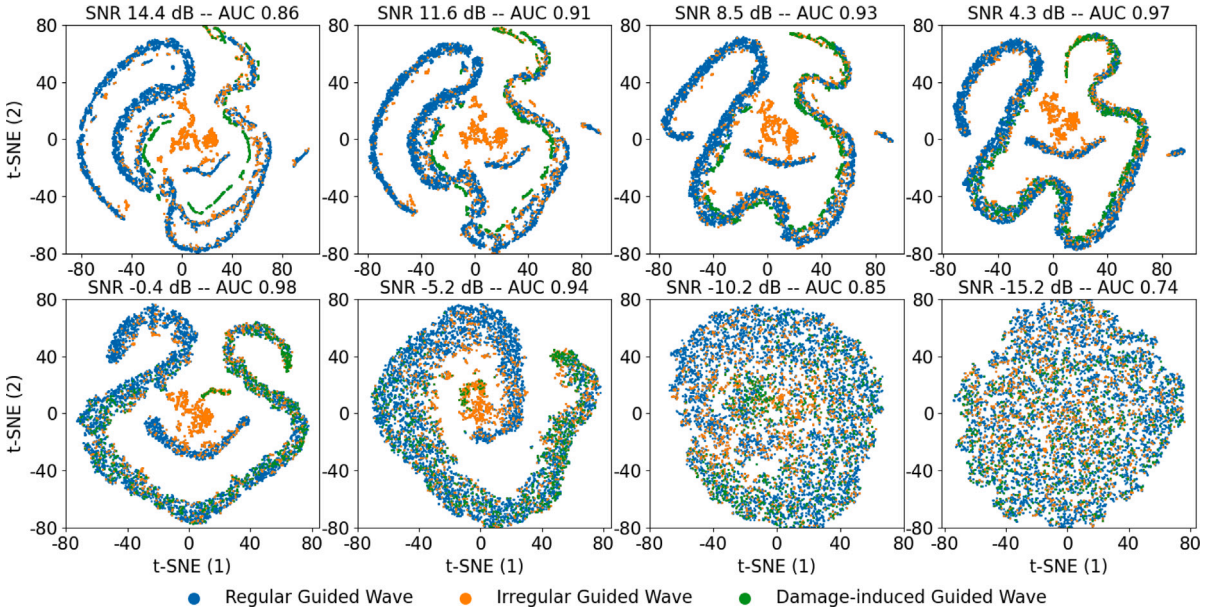

Fig. 15. Each subplot illustrates the distribution of the latent space of the recovery network in a two-dimensional t-SNE plot for the segments of guided waves ranging from 1.2 to 1.3 ms as inputs. The titles of each subplot specify the noise intensity of the white Gaussian noise applied to corrupt the guided waves and the corresponding AUC scores. Distributions of latent space for regular, irregular, and damage-induced guided waves are marked in blue, orange, and green, respectively.

noise into guided waves to modify the noise intensity of input signals (segments of guided waves). Results obtained with both noise-augmentation strategies demonstrate that input signals with relatively low SNR can achieve better damage detection performance, such as around −3 dB, even when the training data contains a significant proportion of damage-induced guided waves. This is because the noise in the input signals increases the neural network's learning difficulty in recovering guided waves from segments. Conversely, excessively strong or weak noise intensities in guided waves degrade damage detection performance. Excessive noise reduces the neural network's ability to learn regular guided waves, leading to increased false alarms, while insufficient noise intensity fails to limit the network's learning ability to recover damage-induced guided waves. The optimal noise intensity of input signals can be estimated based on changes in representative reconstruction coefficients with the SNR of segments of guided waves. An optimal noise intensity is reached at the transition as reconstruction coefficients begin to converge to a single value.

In addition to white Gaussian noise, we also tested white Laplace noise, white Cauchy noise, and pink noise to corrupt the guided wave segments. The results showed that all four types of noise significantly improved damage detection compared to autoencoder-based methods. However, using pink noise required a lower SNR (stronger noise intensity) to achieve a similar AUC score compared to the white noise types. This may be because pink noise has a specific frequency pattern, making it more structured and predictable than uncorrelated noise like white noise. As a result, a higher noise intensity (lower SNR) is needed with pink noise to prevent the recovery network from reconstructing damage-induced guided waves. Additionally, we use t-SNE to visualize the distribution of the recovery network's latent space in two dimensions as the SNR of the input signals (guided wave segments) varied from 14.5 dB to −15.2 dB. The results show that the distribution of irregular guided waves differs significantly from regular and damage-induced guided waves. When the noise intensity reaches suitable levels, such as 4 dB, the separation between regular and damage-induced guided waves becomes clearer, though slightly blurred.

The improvement of the unsupervised damage detection framework with the noise-augmentation strategy is validated using 10 regions of 80-day guided waves collected from uncontrolled and dynamic environmental variations. We intend to explore the applicability of the noise-augmentation strategy to enhance anomaly detection across diverse monitoring systems with other types of time-series signals.

CRediT authorship contribution statement

Kang Yang: Writing – review & editing, Software, Methodology, Investigation, Conceptualization. **Chao Zhang:** Writing – original draft, Methodology. **Hanbo Yang:** Software, Methodology. **Linyuan Wang:** Writing – original draft, Software. **Nam H. Kim:** Writing – review & editing, Methodology. **Joel B. Harley:** Writing – review & editing, Supervision, Project administration, Methodology, Conceptualization.

Declaration of competing interest

The authors declare the following financial interests/personal relationships which may be considered as potential competing interests: Joel B. Harley reports financial support was provided by National Science Foundation. If there are other authors, they declare that they have no known competing financial interests or personal relationships that could have appeared to influence the work reported in this paper.

Acknowledgment

This material is based upon work supported by the National Science Foundation, United States under grant no. EECS-1839704.

Appendix

A.1. Natural SNR estimation

Each segment of the ith guided wave, denoted as $\mathbf{x}_{i,s}$, can be interpreted as the combination of the pure guided wave $\mathbf{x}^r_{i,s}$ and the background noise $\boldsymbol{\eta}$.

$$\mathbf{x}_{i,s} = \mathbf{x}^r_{i,s} + \boldsymbol{\eta} \tag{20}$$

Then, the following equation can be obtained

$$E\{\|\mathbf{x}_{i,s}\|^2\} = E\{\|\mathbf{x}^r_{i,s} + \eta\|^2\} \tag{21}$$

$$= E\{\|\mathbf{x}^r_{i,s}\|^2\} + 2E\{\eta\mathbf{x}^r_{i,s}\} + E\{\|\eta\|^2\} \tag{22}$$

When $E\{\boldsymbol{\eta}\} = 0$ and random variables $\mathbf{x}^r_{i,s}$ and $\boldsymbol{\eta}$ are statistically independent,

$$E\{\eta\mathbf{x}^r_{i,s}\} = E\{\mathbf{x}^r_{i,s}\}E\{\eta\} = 0 \tag{23}$$

Subsequently, the expectation of the squared values for the measured guided wave power can be articulated as

$$E\{\|\mathbf{x}_{i,s}\|^2\} = E\{\|\mathbf{x}^r_{i,s}\|^2\} + E\{\|\boldsymbol{\eta}\|^2\} \tag{24}$$

Then, the estimated natural SNR is

$$SNR_s = 10\log_{10}\frac{P_{\text{signal}}}{P_{\text{noise}}} \tag{25}$$

$$= 10\log_{10}\frac{E\{\|\mathbf{x}_{i,s}\|^2\} - E\{\|\boldsymbol{\eta}\|^2\}}{E\{\|\boldsymbol{\eta}\|^2\}} \tag{26}$$

A.2. Synthetic SNR estimation

The synthetic SNR can be estimated with a similar process as shown in Appendix A.1. A segment of the ith guided wave with additional noise, denoted as $\mathbf{x}_{i,s}$, can be interpreted as the combination of the pure guided wave $\mathbf{x}^r_{i,s}$, the background noise $\boldsymbol{\eta}$ and additional Gaussian noise ε.

$$\mathbf{x}^{\mathcal{N}}_{i,s} = \mathbf{x}^r_{i,s} + \eta + \varepsilon \tag{27}$$

Then, given that the random variables $\mathbf{x}^r_{i,s}$, the background noise $\boldsymbol{\eta}$, and the additional Gaussian noise ε are statistically independent, and $E\{\boldsymbol{\eta}\} = 0$ and $E\{\boldsymbol{\varepsilon}\} = 0$, we can obtain

$$\begin{aligned} E\{\|\mathbf{x}^{\mathcal{N}}_{i,s}\|^2\} &= E\{\|\mathbf{x}^r_{i,s} + \eta + \varepsilon\|^2\} && (28)\\ &= E\{\|\mathbf{x}^r_{i,s}\|^2 + \|\eta\|^2 + \|\varepsilon\|^2 + 2\mathbf{x}^r_{i,s}\eta + 2\varepsilon\mathbf{x}^r_{i,s} + 2\eta\varepsilon\} && (29)\\ &= E\{\|\mathbf{x}^r_{i,s}\|^2\} + E\{\|\eta\|^2\} + E\{\|\varepsilon\|^2\} + 2E\{\mathbf{x}^r_{i,s}\}E\{\eta\} + 2E\{\varepsilon\}E\{\mathbf{x}^r_{i,s}\} + 2E\{\eta\}E\{\varepsilon\} && (30)\\ &= E\{\|\mathbf{x}^r_{i,s}\|^2\} + E\{\|\eta\|^2\} + E\{\|\varepsilon\|^2\} && (31) \end{aligned}$$

Therefore, the estimation of synthetic SNR can be attained as

$$\begin{aligned} SNR^{\mathcal{N}}_s &= 10\log_{10}\frac{P_{\text{signal}}}{P_{\text{noise + Gaussian noise}}} && (32)\\ &= 10\log_{10}\frac{E\{\|\mathbf{x}_{i,s}\|^2\} - E\{\|\boldsymbol{\eta}\|^2\}}{E\{\|\boldsymbol{\eta}\|^2\} + E\{\|\boldsymbol{\varepsilon}\|^2\}} && (33) \end{aligned}$$

Data availability

Data will be made available on request.

References

[1] P. Wang, W. Zhou, H. Li, A singular value decomposition-based guided wave array signal processing approach for weak signals with low signal-to-noise ratios, Mech. Syst. Signal Process. 141 (2020) 106450.
[2] M. Eybpoosh, M. Berges, H.Y. Noh, An energy-based sparse representation of ultrasonic guided-waves for online damage detection of pipelines under varying environmental and operational conditions, Mech. Syst. Signal Process. 82 (2017) 260–278.
[3] Y. Du, S. Zhou, X. Jing, Y. Peng, H. Wu, N. Kwok, Damage detection techniques for wind turbine blades: A review, Mech. Syst. Signal Process. 141 (2020) 106445.
[4] M. Hong, Q. Wang, Z. Su, L. Cheng, In situ health monitoring for bogie systems of CRH380 train on Beijing–Shanghai high-speed railway, Mech. Syst. Signal Process. 45 (2) (2014) 378–395.
[5] J. Segers, S. Hedayatrasa, G. Poelman, W. Van Paepegem, M. Kersemans, Robust and baseline-free full-field defect detection in complex composite parts through weighted broadband energy mapping of mode-removed guided waves, Mech. Syst. Signal Process. 151 (2021) 107360.
[6] H. Lee, H.J. Lim, T. Skinner, A. Chattopadhyay, A. Hall, Automated fatigue damage detection and classification technique for composite structures using lamb waves and deep autoencoder, Mech. Syst. Signal Process. 163 (2022) 108148.
[7] J. Mao, H. Wang, B.F. Spencer Jr., Toward data anomaly detection for automated structural health monitoring: Exploiting generative adversarial nets and autoencoders, Struct. Health Monit. 20 (4) (2021) 1609–1626.
[8] L. Lomazzi, R. Junges, M. Giglio, F. Cadini, Unsupervised data-driven method for damage localization using guided waves, Mech. Syst. Signal Process. 208 (2024) 111038.
[9] B. Zhang, X. Hong, Y. Liu, Deep convolutional neural network probability imaging for plate structural health monitoring using guided waves, IEEE Trans. Instrum. Meas. 70 (2021) 1–10.
[10] V. Giurgiutiu, Structural Health Monitoring: with Piezoelectric Wafer Active Sensors, Elsevier, 2007.
[11] G. Li, A. Chattopadhyay, Multi-dimensional signal processing and mode tracking approach for guided wave based damage localization in X-COR sandwich composite, Mech. Syst. Signal Process. 109 (2018) 134–149.
[12] A. Stawiarski, The nondestructive evaluation of the GFRP composite plate with an elliptical hole under fatigue loading conditions, Mech. Syst. Signal Process. 112 (2018) 31–43.
[13] C.L. Wilson, F.K. Chang, Monitoring fatigue-induced transverse matrix cracks in laminated composites using built-in acousto-ultrasonic techniques, Struct. Health Monit. 15 (3) (2016) 335–350.
[14] C. Liu, J.B. Harley, M. Bergés, D.W. Greve, I.J. Oppenheim, Robust ultrasonic damage detection under complex environmental conditions using singular value decomposition, Ultrasonics 58 (2015) 75–86.
[15] J.B. Harley, J.M. Moura, Scale transform signal processing for optimal ultrasonic temperature compensation, IEEE Trans. Ultrason. Ferroelectr. Freq. Control 59 (10) (2012) 2226–2236.
[16] J. Moll, R. Schulte, B. Hartmann, C. Fritzen, O. Nelles, Multi-site damage localization in anisotropic plate-like structures using an active guided wave structural health monitoring system, Smart Mater. Struct. 19 (4) (2010) 045022.
[17] S.C. Olisa, M.A. Khan, A. Starr, Review of current guided wave ultrasonic testing (GWUT) limitations and future directions, Sensors 21 (3) (2021) 811.
[18] H. Sohn, Effects of environmental and operational variability on structural health monitoring, Phil. Trans. R. Soc. A 365 (1851) (2007) 539–560.
[19] C. Su, M. Jiang, S. Lv, S. Lu, L. Zhang, F. Zhang, Q. Sui, Improved damage localization and quantification of CFRP using lamb waves and convolution neural network, IEEE Sens. J. 19 (14) (2019) 5784–5791.

[20] V. Ewald, R.M. Groves, R. Benedictus, DeepSHM: A deep learning approach for structural health monitoring based on guided lamb wave technique, in: Sensors and Smart Structures Technologies for Civil, Mechanical, and Aerospace Systems 2019, Vol. 10970, SPIE, 2019, pp. 84–99.
[21] S. Zhang, C.M. Li, W. Ye, Damage localization in plate-like structures using time-varying feature and one-dimensional convolutional neural network, Mech. Syst. Signal Process. 147 (2021) 107107.
[22] L. Lomazzi, S. Fabiano, M. Parziale, M. Giglio, F. Cadini, On the explainability of convolutional neural networks processing ultrasonic guided waves for damage diagnosis, Mech. Syst. Signal Process. 183 (2023) 109642.
[23] M. Rautela, J. Senthilnath, E. Monaco, S. Gopalakrishnan, Delamination prediction in composite panels using unsupervised-feature learning methods with wavelet-enhanced guided wave representations, Compos. Struct. 291 (2022) 115579.
[24] V. Malviya, I. Mukherjee, S. Tallur, Edge-compatible convolutional autoencoder implemented on FPGA for anomaly detection in vibration condition-based monitoring, IEEE Sensors Lett. 6 (4) (2022) 1–4.
[25] Z. Wang, Y.-J. Cha, Unsupervised deep learning approach using a deep auto-encoder with a one-class support vector machine to detect damage, Struct. Health Monit. 20 (1) (2021) 406–425.
[26] M. Sanayei, A. Khaloo, M. Gul, F.N. Catbas, Automated finite element model updating of a scale bridge model using measured static and modal test data, Eng. Struct. 102 (2015) 66–79.
[27] M. Rautela, E. Monaco, S. Gopalakrishnan, Delamination detection in aerospace composite panels using convolutional autoencoders, in: Health Monitoring of Structural and Biological Systems XV, Vol. 11593, SPIE, 2021, pp. 292–301.
[28] O. Avci, O. Abdeljaber, S. Kiranyaz, M. Hussein, M. Gabbouj, D.J. Inman, A review of vibration-based damage detection in civil structures: From traditional methods to machine learning and deep learning applications, Mech. Syst. Signal Process. 147 (2021) 107077.
[29] J.K. Chow, Z. Su, J. Wu, P.S. Tan, X. Mao, Y.-H. Wang, Anomaly detection of defects on concrete structures with the convolutional autoencoder, Adv. Eng. Inform. 45 (2020) 101105.
[30] S. Sawant, S. Patil, J. Thalapil, S. Banerjee, S. Tallur, Temperature variation compensated damage classification and localisation in ultrasonic guided wave SHM using self-learnt features and Gaussian mixture models, Smart Mater. Struct. 31 (5) (2022) 055008.
[31] S. Sawant, A. Sethi, S. Banerjee, S. Tallur, Unsupervised learning framework for temperature compensated damage identification and localization in ultrasonic guided wave SHM with transfer learning, Ultrasonics 130 (2023) 106931.
[32] P. Kashyap, K. Shivgan, S. Patil, B.R. Raja, S. Mahajan, S. Banerjee, S. Tallur, Unsupervised deep learning framework for temperature-compensated damage assessment using ultrasonic guided waves on edge device, Sci. Rep. 14 (1) (2024) 3751.
[33] J. Moll, J. Kathol, C.-P. Fritzen, M. Moix-Bonet, M. Rennoch, M. Koerdt, A.S. Herrmann, M.G. Sause, M. Bach, Open guided waves: online platform for ultrasonic guided wave measurements, Struct. Health Monit. 18 (5–6) (2019) 1903–1914.
[34] M. Rautela, S. Jayavelu, J. Moll, S. Gopalakrishnan, Temperature compensation for guided waves using convolutional denoising autoencoders, in: Health Monitoring of Structural and Biological Systems XV, Vol. 11593, SPIE, 2021, pp. 316–326.
[35] M. Rautela, J. Senthilnath, J. Moll, S. Gopalakrishnan, Combined two-level damage identification strategy using ultrasonic guided waves and physical knowledge assisted machine learning, Ultrasonics 115 (2021) 106451.
[36] T. Peng, A. Saxena, K. Goebel, Y. Xiang, S. Sankararaman, Y. Liu, A novel Bayesian imaging method for probabilistic delamination detection of composite materials, Smart Mater. Struct. 22 (12) (2013) 125019.
[37] V. Memmolo, L. Maio, N.D. Boffa, E. Monaco, F. Ricci, Damage detection tomography based on guided waves in composite structures using a distributed sensor network, Opt. Eng., Bellingham 55 (1) (2016) 011007.
[38] J. An, S. Cho, Variational autoencoder based anomaly detection using reconstruction probability, Special Lecture on IE 2 (1) (2015) 1–18.
[39] A. Abbassi, N. Römgens, F.F. Tritschel, N. Penner, R. Rolfes, Evaluation of machine learning techniques for structural health monitoring using ultrasonic guided waves under varying temperature conditions, Struct. Health Monit. 22 (2) (2023) 1308–1325.
[40] K. Yang, S. Kim, J.B. Harley, Unsupervised long-term damage detection in an uncontrolled environment through optimal autoencoder, Mech. Syst. Signal Process. 199 (2023) 110473.
[41] M. Sakurada, T. Yairi, Anomaly detection using autoencoders with nonlinear dimensionality reduction, in: Proceedings of the MLSDA 2014 2nd Workshop on Machine Learning for Sensory Data Analysis, 2014, pp. 4–11.
[42] N.V. Chawla, N. Japkowicz, A. Kotcz, Special issue on learning from imbalanced data sets, ACM SIGKDD Explor. Newsl. 6 (1) (2004) 1–6.
[43] C. Tian, L. Fei, W. Zheng, Y. Xu, W. Zuo, C.-W. Lin, Deep learning on image denoising: An overview, Neural Netw. 131 (2020) 251–275.
[44] J. Guan, R. Lai, A. Xiong, Wavelet deep neural network for stripe noise removal, IEEE Access 7 (2019) 44544–44554.
[45] T. Pang, H. Zheng, Y. Quan, H. Ji, Recorrupted-to-recorrupted: unsupervised deep learning for image denoising, in: Proceedings of the IEEE/CVF Conference on Computer Vision and Pattern Recognition, 2021, pp. 2043–2052.
[46] M. Rautela, S. Gopalakrishnan, Ultrasonic guided wave based structural damage detection and localization using model assisted convolutional and recurrent neural networks, Expert Syst. Appl. 167 (2021) 114189.
[47] Z. Chen, C.K. Yeo, B.S. Lee, C.T. Lau, Autoencoder-based network anomaly detection, in: 2018 Wireless Telecommunications Symposium, WTS, IEEE, 2018, pp. 1–5.
[48] K. Yang, S. Kim, J.B. Harley, Improving long-term guided wave damage detection with measurement resampling, IEEE Sens. J. (2023).
[49] K. Yang, S. Kim, R. Yue, H. Yue, J.B. Harley, Long-term guided wave structural health monitoring in an uncontrolled environment through long short-term principal component analysis, Struct. Health Monit. 21 (4) (2022) 1501–1517.
[50] C. Liu, J. Dobson, P. Cawley, Efficient generation of receiver operating characteristics for the evaluation of damage detection in practical structural health monitoring applications, Proc. R. Soc. A 473 (2199) (2017) 20160736.
[51] S. Kim, S. Shiveley, A.C.S. Douglass, Y. Zhang, R. Sahay, D.O. Adams, J.B. Harley, Efficient storage and processing of large guided wave data sets with random projections, Struct. Health Monit. (2020) 1475921720960196.
[52] S. Heinlein, P. Cawley, T. Vogt, Validation of a procedure for the evaluation of the performance of an installed structural health monitoring system, Struct. Health Monit. 18 (5–6) (2019) 1557–1568.
[53] P. Paialunga, J. Corcoran, Damage detection in guided wave structural health monitoring using Gaussian process regression, Struct. Health Monit. (2023) 14759217231159399.
[54] J. Liang, D. Hu, J. Feng, Do we really need to access the source data? source hypothesis transfer for unsupervised domain adaptation, in: International Conference on Machine Learning, PMLR, 2020, pp. 6028–6039.